Eur. Phys. J. D (2014) 68: 188
DOI: 10.1140/epjd/e2014-50342-9

THE EUROPEAN PHYSICAL JOURNAL D

Colloquium

One hundred years of the Franck-Hertz experiment

Robert E. Robson[1,2,a], Ronald D. White[1], and Malte Hildebrandt[3]

[1] School of Engineering and Physical Sciences, James Cook University, Townsville, QLD 4811, Australia
[2] Research School of Physical Science & Engineering, Australian National University, Canberra, Australia
[3] Paul Scherrer Institute, Laboratory for Particle Physics, 5232 Villigen PSI, Switzerland

Received 30 April 2014 / Received in final form 30 May 2014
Published online 18 July 2014 – © EDP Sciences, Società Italiana di Fisica, Springer-Verlag 2014

Abstract. The 1914 experiment of James Franck and Gustav Hertz provided a graphic demonstration of quantization properties of atoms, thereby laying the foundations of modern atomic physics. This article revisits the experiment on the occasion of its Centenary, compares traditional and modern interpretations, and focuses in particular on the link between microscopic processes, which are governed by the laws of quantum mechanics, and macroscopic phenomena as measured in the laboratory. A goal is to place the physics underlying the operation of the Franck-Hertz experiment within the context of contemporary gaseous electronics, and to that end we reach back even further in time to the 1872 kinetic equation of Ludwig Boltzmann. We also show how the experiment can be modelled using fluid equations and Monte Carlo simulation, and go further to show how non-local effects, resonances and striations in plasmas have much in common with the electron physics in the drift region of the Franck-Hertz experiment.

1 Introduction

1.1 The Franck-Hertz experiment and modern atomic physics

The famous late nineteenth and early twentieth century experiments based on investigations of electrical currents in gases laid the foundations of modern physics [1–3], and pre-eminent among these is the seminal experiment of Franck and Hertz [4], the subject of the present review and of a recent shorter article [5]. The results of the experiment (see Figs. 1 and 2) were reported 100 years ago, and are generally regarded as confirming the model of the atom which Bohr had proposed a year earlier. The experiment is traditionally considered in the context of single-scattering atomic collision physics, with scant regard paid to the statistical mechanics necessary to describe the behaviour of many electrons undergoing many collisions with gas atoms, en route from the cathode to the anode. In particular, the periodic structures which develop in the drift region, which are key to the operation of the experiment, must be more carefully analysed in order to be able to correctly interpret the experiment. These structures are in fact similar in origin to the "luminous layers" observed firstly by Holst and Oosterhuis [6], and subsquently by others [7–10], including an investigation by Fletcher and Purdie [11,12] in a Steady state Townsend experiment. However, a thorough understanding of the basic physics of these periodic structures has emerged only recently, through the kinetic theory of gases, allowing the Franck-Hertz experiment to be finally interpreted rigorously after almost 100 years. The details are reported in this colloquium.

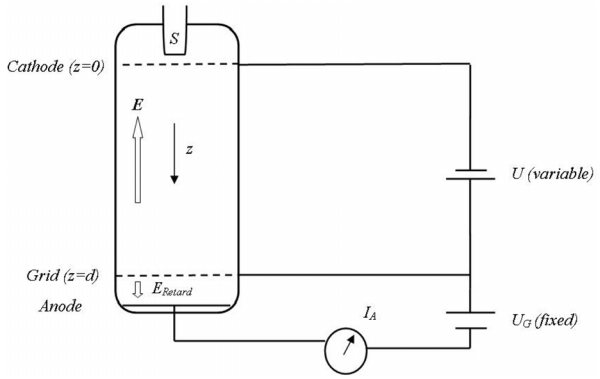

Fig. 1. Schematic representation of the Franck-Hertz experiment, with the gas under investigation filling the region between plane-parallel electrodes. Electrons emitted from the source S move under the influence of a uniform field $E = U/d$ in the region $0 \leqslant z \leqslant d$ between cathode and grid. Beyond the grid at $z = d$ the retarding voltage U_G allows only electrons with energies above eU_G to contribute to the anode current I_A. The voltage U is increased and the resulting I_A-U curve is recorded, as in Figures 2 and 4 for Hg vapour and Ne gas, respectively.

At the outset we emphasise that the classic Franck-Hertz apparatus involves the passage of low current, low density electrons through a gas, and may therefore be categorised as a "swarm" experiment [1,13–16]. No space-charge or plasma effects are apparent, and the operation of the experiment is underpinned by "natural" or "free"

[a] e-mail: robert.robson@anu.edu.au

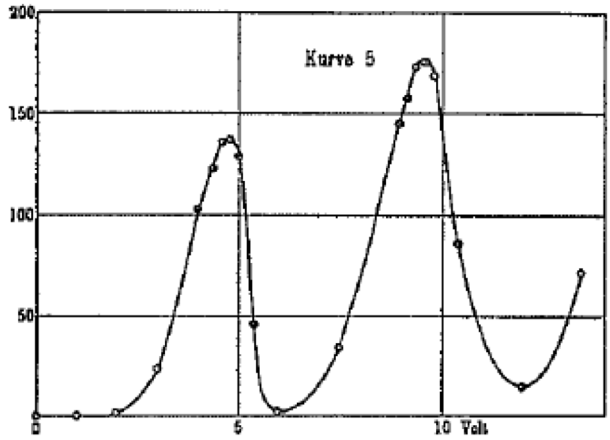

Fig. 2. The current-voltage characteristic for Hg vapour reported by Franck-Hertz experiment [4] for which the voltage difference between peak currents is $\Delta U = 4.9$ V.

oscillations of average electron properties. On the other hand, periodic electron structures called "striations" arise from a synergy between "natural" or "Franck-Hertz" oscillations and plasma effects, due to the presence of both ions and electrons, and are ubiquitous in gas discharges at higher currents [3,17–25]. The picture is complicated by a spatially varying, self-consistent space charge field, in contrast to the externally imposed, constant field in the Franck-Hertz experiment. The phenomenon was first reported over 170 years ago by Abria [17] (and perhaps observed even earlier by Michael Faraday [3]) and is considered to have inspired the subsequent ground-breaking experiments involving gas discharges, which in turn led to the era of modern physics. It is therefore ironic to note that while physics per se has made enormous strides in the past century, a complete understanding of striations is still lacking. We shall return to this theme in the closing stages of this paper.

Nowadays the Franck-Hertz experiment is available off-the-shelf commercially. It has been *de rigueur* in the undergraduate laboratory for several generations of physicists, who have been raised on the highly simplified explanations of standard textbooks [26,27] and, nowadays, innumerable internet web sites. While the wider physics community has, possibly for this reason, tended to regard the experiment as being useful for pedagogical purposes only, it has been realised recently [28] that there is still much basic physics to be investigated, e.g., the effect of elastic (e, Hg) collisions [29,30]. On the occasion of the Centenary of the Franck-Hertz experiment we feel it is only appropriate to explore the true extent of the physics it reveals.

Before embarking on the main task, however, it is helpful to add some historical context.

1.2 Historical and biographical notes

James Franck [31,32] and Gustav Hertz [33] commenced their collaboration in 1911 in Berlin, and for the next three years investigated the interactions of slow electrons with neutral gases [34]. They were aiming at a "general kinetic theory of electrons in gases", as Franck did not agree with Townsend's explanation of electron scattering processes in gas discharge drift tubes. Franck and Hertz improved on existing experimental methods, which were used, amongst others, by Philipp Lenard for investigating the properties of cathode rays in low density gases. This ultimately led to the 1914 seminal investigation in mercury vapour [4] which is commonly referred to as *the* "Franck-Hertz experiment", although variations do exist [35,36]. The results were first interpreted as an indication of the ionisation voltage of mercury vapour, but from a subsequent experiment measuring light emission, they concluded that it was in fact a determination of an excitation level of the mercury atom. For their experiment, which provided a graphic illustration of the quantisation of atomic energy levels, Franck and Hertz received the 1925 Nobel Prize [37]. Brief biographies follow.

James Franck [31,32] was born in Hamburg in 1882, and lived in the neighbourhood of the present University of Hamburg. He first went to Heidelberg to study law, switched to science and mathematics, and then transferred to the Friedrich-Wilhelms-Universität of Berlin, where he obtained a doctorate in experimental physics in 1906. It was here that he teamed up with Gustav Hertz, also originally from Hamburg, to carry out their seminal experiment of 1914, which, as noted above, brought them the 1925 Nobel Prize for Physics. By then he was established as Professor of Physics at the University of Göttingen, where he led a vibrant and very influential department. However he subsequently left Germany for the USA. He is also well known for the Franck-Condon principle, and for his views on the use of atomic weapons. He died in Göttingen in 1964.

Gustav Hertz [33], a nephew of Heinrich Hertz, was born in Hamburg in 1887. He studied physics and mathematics in Göttingen, Munich and at the Friedrich-Wilhelms-Universität in Berlin where he finished with his doctoral thesis in 1911. At the physics institute in Berlin he met James Franck, and together they started work on a series of measurements which ultimately led to the famous experiment described in this article. Hertz habilitated in 1917 and he became a professor at the Universities of Halle, Berlin and finally Leipzig. He also worked at several industrial research laboratories, notably Philips[1] and Siemens. Hertz retired in 1961 and died in 1975 in Berlin.

Ludwig Boltzmann (1844–1906) [39] also figures prominently in this article, through his famous 1872 kinetic equation [40,41], which to this day underpins the analysis of many non-equilibrium systems, and which is

[1] The Natuurkundig Laboratorium der N.V. Philips Gloeilampenfabrieken, Eindhoven, Holland, was one of the leading industrial research laboratories in the world, in particular in the field of gas discharges during the first half of the 20th century [38]. The significant work of Holst, Oosterhuis, Druyvesteyn and Penning [7–9] was performed at this laboratory.

eminently suitable for understanding electron properties in the Franck-Hertz drift tube. Note, however, that there is no evidence that Franck and Hertz were significantly influenced by Boltzmann's ideas at the time of their experiment, even though one of Franck's early collaborators in Berlin was Lise Meitner, who had been a student of Boltzmann in Vienna.

1.3 Related physical phenomena and experiments

The Franck-Hertz experiment provides a graphic illustration of the quantisation of atomic energy levels, through the generation of an oscillatory anode current in an external circuit including a control grid in front of the anode (Fig. 1). This external periodic behaviour reflects an internal periodic electron structure within the drift tube, of whose physical origins are in fact similar to those observed in other experimental arrangements:

(a) If the grid in front of the anode in Figure 1 were removed, the apparatus could be thought of as a type of steady state Townsend "swarm" experiment, and as such, contact can be usefully made with the swarm physics literature [1,13–16]. Fletcher and Purdie [11,12] have pointed out that periodic structures in such low current, low pressure discharges have long been known [6,7,10,42–44], dating back to the 1920s. They employed the photon flux technique to observe periodic electron properties in several noble gases, directly and non-intrusively. Fletcher also showed that the oscillations were damped through the addition of only a few per cent molecular gas, and concluded that a sufficiently large gap between the ground state and the first excited states is required to produce oscillations. This is also the reason why the Franck-Hertz experiment is considered to operate satisfactorily only with monatomic gases (there are exceptions, which we shall discuss later).

(b) A number of articles in the modern low temperature plasma literature dealing with spatial inhomogeneity [45–53] report on damped periodic structures. The work of Winkler and collaborators [48–50] has demonstrated pronounced sensitivity to E/n_0 (the ratio of the field to the gas number density), and has shown that it is only in a "window" of *intermediate* fields that periodicity is observed. The explanation given in reference [50] essentially follows the classical Franck-Hertz argument (without acknowledging the connection) and also confirms Fletcher's suggestion [11] that increasing the number of inelastic channels enhances damping. Reference [50] is particularly noteworthy for introducing a "multiterm" analysis of Boltzmann's equation capable of dealing with spatial inhomogeneity, in contrast to the severe limitations which many authors place on their work by unnecessarily limiting the representation of the electron velocity distribution function to the first two terms of an expansion in spherical harmonics. It is to be emphasised that while references [47–50], and others, go on to deal with inhomogeneous fields and space charge phenomena, this is not in any way connected with the effects we are presently discussing.

(c) A modern view [54] is that *all* swarm experiments can be analysed from a common standpoint, in which a generalised eigenvalue equation, deriving from the Boltzmann equation, and an associated "dispersion relation", furnish all quantities of physical interest. If, as we argue, the Franck-Hertz experiment can be thought of as belonging to the steady state Townsend category, then the full weight of modern eigenvalue theory [54,55] can be brought to bear. This is most useful for dealing with the asymptotic region far downstream from the source, where the eigenvalue with the lowest real part controls the spatial structure, but the full profile can also be calculated by numerical solution of the Boltzmann equation [30,56].

It is evident that in reviewing the classic Franck-Hertz experiment we can profitably link together several seemingly disparate strands of the literature, both modern and traditional, and at the same time discuss some very rich and interesting physical phenomena.

1.4 Structure of this review

In Section 2 we review the experiment and the traditional interpretation of results for both Hg and Ne, and also look at periodic structures directly measured in a steady state Townsend experiment with Ne. Section 3 outlines the theoretical requirements needed to interpret the experiment and in Sections 4 and 5 we discuss the Boltzmann equation and fluid equation analysis, respectively. Numerical calculations are given for a simple cross section model in the first instance, and then with real cross section models for mercury vapour and neon gas, the latter using a Monte Carlo simulation. In Section 6 we give a brief discussion of non-local effects and resonances with Franck-Hertz waves, and conclude by returning to the subject of striations, which we regard as the progenitor of gas discharge experiments.

2 The experiment

2.1 Apparatus and original results

Figure 1 shows a schematic representation of the experiment in plane parallel geometry, which is nowadays favoured over the cylindrical arrangement originally used by Franck and Hertz. Electrons are emitted at a steady rate from the cathode into a drift tube containing an atomic gas of number density n_0, and are scattered in collisions with gas atoms (both elastic and inelastic) as they fall through a voltage U over a distance d to the control grid. The retarding voltage U_G applied between grid and anode allows only higher energy electrons to contribute to the measured anode current I_A. An oscillatory I_A-U curve is observed, and the spacing between peaks, designated by ΔU, is supposed to be directly related to some quantised atomic energy level.

The results of the original experiment using mercury vapour published in 1914 are shown in three different I_A-U curves in reference [4], with the best known of these reproduced in Figure 2, showing $\Delta U \approx 4.9$ V.

As already mentioned, Franck and Hertz initially interpreted this as the ionisation potential of a mercury atom, but after a subsequent experiment they concluded that their result indicated an electronic excitation level of energy $\varepsilon_I = e\Delta U = 4.9$ eV. In addition, they observed that radiation emitted from excited atoms returning to their ground state had a wavelength $\lambda = 253.6$ nm. This, together with $\varepsilon_I = hc/\lambda$, could be used to either: (i) confirm the measured value of ε_I, or (ii) provide an independent estimate of Planck's constant h.

At first Franck and Hertz were not aware of the Bohr model, and only appreciated the full implications of their results several years later, in what was in fact their last joint publication [57]. On the other hand Bohr himself realized already in 1915 the importance of the Franck-Hertz experiment as confirming his quantised model of the atom [58].

2.2 The traditional model

Within a certain range of voltages and gas pressures the mean electron energy profile $\varepsilon(z)$ is oscillatory in the drift region between cathode and grid. Such a spatially periodic structure is a macroscopic reflection of atomic quantisation and, while observed directly in other experiments [11,12], it is usually modelled somewhat crudely for the Franck-Hertz experiment. Thus the traditional textbook model has each electron starting from rest at the cathode, and accelerated by the electric field $E = U/d$ until it achieves sufficient energy to excite a gas atom to some quantised energy level ε_I. The electron then gives up all its energy abruptly in an inelastic collision, and is again accelerated from rest to energy ε_I, when it is once more brought to rest in a collision, and so on. The average electron energy $\varepsilon(z)$ (which is the energy of each and every electron in this model viz., a unidirectional monoenergetic electron "beam") thus fluctuates as a function of the distance z downstream from the source in a sharp, "saw tooth" fashion with spatial period $\Delta z = \varepsilon_I/eE$.

The text book model goes on to say that as U (and therefore E) is increased, Δz decreases, i.e., the pattern shrinks, and the electron energy at the grid $\varepsilon(d)$ rises and falls accordingly. If $\varepsilon(d) > U_G$, electrons can pass to the anode, and hence the anode current I_A should rise and fall as U increases.

Since an increase in voltage of

$$\Delta U = \varepsilon_I/e \tag{1}$$

produces exactly one more additional internal oscillation, this must be the voltage separation between current peaks. This result is actually valid for *any* oscillatory profile $\varepsilon(z)$, not just the saw tooth model of the textbooks, though as we shall see, the energy wavelength $\varepsilon_I = eE\Delta z$ will not in general correspond exactly to a quantised atomic energy level.

Table 1. Threshold energies and approximate maximum cross sections for excitation of Hg to the energy levels shown by inelastic collisions (two numbers indicate two peaks of the cross section as seen in Fig. 3).

J	Process	Threshold (eV)	Maximum cross section (10^{-20} m^2)
0	$6s6p\ ^3P_0$	4.67	0.4/0.5
1	$6s6p\ ^3P_1$	4.89	3.5/5.0
2	$6s6p\ ^3P_2$	5.46	4.0

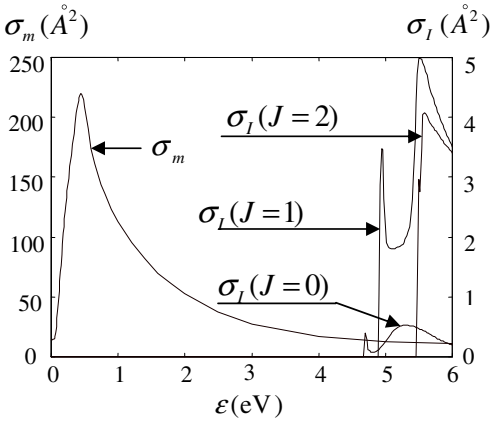

Fig. 3. The momentum transfer cross section σ_m and three inelastic cross sections σ_I for electron scattering from mercury [29,59]. See Table 1 for an explanation of notation.

2.3 Experimental results and questions of interpretation

2.3.1 *Mercury*

The textbook interpretation of Figure 2 suggests the Hg atom therefore has a quantised energy level of 4.9 eV. This is indeed close to 4.89 eV, the energy of the *second* quantised state (the 6 $^1S_0 \rightarrow 6\ ^3P_1$ transition), but the *first* quantised level of Hg, for which $\varepsilon_I = 4.67$ eV (the 6 $^1S_0 \rightarrow 6\ ^3P_0$ transition – see Tab. 1) seems to be bypassed. Since this lowest level is metastable, one would not expect to see any corresponding spectral emission line, but why should it not affect the I_A-U curve? The question was addressed by Hanne [59], who pointed out that the cross section for excitation of the first excited level of Hg is small (see Tab. 1 and Fig. 3).

One must look further, however, to understand why the 6 $^1S_0 \rightarrow 6\ ^3P_2$ process, with threshold energy 5.46 eV, does not appear to significantly influence the measurement.

2.3.2 *Neon*

The experimental apparatus for neon is readily available commercially "off the shelf" from Leybold Didactic[2]. The

[2] http://www.ld-didactic.de/literatur/hb/e/p6/p6243_e.pdf

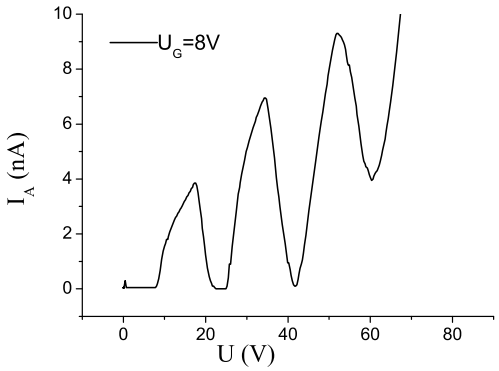

Fig. 4. Measured Franck-Hertz I_A-U curve for neon using a Leybold Didactic GmbH apparatus.

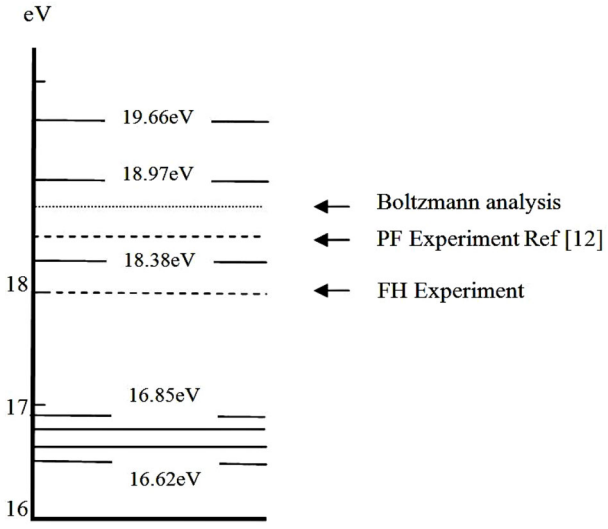

Fig. 5. Energy level diagram for neon (solid lines), experimentally measured values of ε_I (dashed lines) from photon flux experiment (PF), Franck-Hertz experiment (FH) and theoretically calculated value of ε_I from Boltzmann equation analysis (dotted line).

measured current-voltage characteristic is shown in Figure 4 which, together with the text book model, suggests that the neon atom has an energy level $\varepsilon_I = e\Delta U \approx 18 \pm 1$ eV. Even if this were taken as a reflection of the $^3S_1$ level of energy 18.4 eV alone (and we do not believe this is the case), the same question would arise as for Hg: why should the experiment appear to register excitation of one particular level, and bypass others (see Fig. 5)? An inspection of the (e, Ne) cross section data, shown in abbreviated form in Table 2, shows why we cannot use the same argument as for Hg to dismiss the effects of other inelastic channels. Hence we must look for another interpretation of the measured value of ε_I.

The laboratory manual accompanying the Leybold apparatus at least acknowledges the problem, and suggests that an element of "probability" comes into play. In physical terms, this means that the cross sections for each of the possible processes must be accounted for.

Table 2. Threshold energies and approximate maximum cross sections for excitation of neon to the energy levels shown by inelastic collisions [60]. See Figure 11 for the detailed electron – neon cross-sections.

Process	Threshold (eV)	Maximum cross section (10^{-20} m^2)
$2p^5 3s\ ^3P_2$	16.62	0.01
$2p^5 3s\ ^3P_1$	16.67	0.012
$2p^5 3s\ ^3P_0$	16.72	0.0024
$2p^5 3s\ ^1P_1$	16.85	0.12
$2p^5 3p\ ^3S_1$	18.38	0.033
$2p^5 3p\ ^2P$	18.97	0.026
$2p^5 4s\ ^2S$	19.66	0.033

2.3.3 *Argon*

Recently Magyar et al. [61] have described a Franck-Hertz experiment in argon gas, with electrons generated by photoemission at the source, instead of the usual thermionic emission. An important feature of the experimental arrangement is the ability to vary gas pressure (from 25 to 400 Pa), a facility in common with swarm experiments, and which has an effect similar to varying the length of the drift region [13–16]. At the highest pressure, electrons arrive at the grid with minimal residual memory of the source, and the current reflects the intrinsic properties of the gas atoms, as desired. This is discussed in more detail in Section 4.3. From their figure 3e, for which gas pressure is highest, and the waveform most regular, we estimate that $\Delta U = 12 \pm 1$ V. From their figure 5g, which shows the calculated mean energy within the drift region as a function of position, we estimate the energy wavelength to be $\varepsilon_I = eE\Delta z \approx 12$ eV, which is consistent with equation (1). As observed for neon, the measured value of ε_I does not appear to correspond to any single energy level of an argon atom [62].

2.4 A critical re-examination of the basic physics in the drift region

The fundamental question which has emerged is this:

How is the value of ε_I measured in the Franck-Hertz experiment to be interpreted in terms of the quantised energy levels of the atoms comprising the gas?

The answer requires a review of the basic physics of electrons in the drift region.

Firstly, note that *elastic scattering* is important, e.g., the elastic momentum transfer cross section in Hg is enormous (∼50 times the magnitudes of the inelastic cross-sections – see Fig. 3), and electrons in the drift region therefore may make many elastic collisions before exciting an atom in an inelastic collision. There are two main effects:

(i) Elastic collisions randomise the *directions* of electron velocities, and hence the electron velocity distribution function $f(z, \mathbf{v})$ is nearly isotropic in the drift region; and

(ii) Although electrons exchange (i.e., lose or gain) only a small fraction $\sim 2m/m_0$ of energy in elastic collisions with atoms of a much larger mass m_0, the net effect after many such collisions is to create a large spread of energies about the mean energy.

Thus in the drift region of a Franck-Hertz experiment, $f(z, \mathbf{v})$ is both broad in energy and nearly *isotropic* in velocity space [30]. Electrons behave like a *swarm* [1,13–16], quite the opposite of a unidirectional, mono-energetic beam, as the textbook model would have us believe. This means that several inelastic channels may be open simultaneously, and that the measured value of ε_I can be expected to reflect a number atomic energy levels, weighted by the electron energy distribution function.

2.5 Direct observation of periodic structures

Periodic electron structures have for long been known in gaseous electronics, but the Franck-Hertz experiment is not normally considered to be part of this literature, in spite of some clear connections. Thus the *steady state Townsend (SST)* "swarm" experiment [1,11–13], can be thought of as representing the drift tube region of Figure 1, where atoms are excited by electron impact. However, there is no grid and no measurement of currents in an external circuit. Instead, Fletcher [11] and Fletcher and Purdie [12] investigated the spatial profile of electrons in noble gases *directly* and *non-intrusively* by measuring the intensity of photons emitted in de-excitation of atoms, in the so-called "photon flux technique".

2.5.1 *Neon*

Profiles obtained for neon in reference [12] are reproduced in Figure 6, from which the authors estimated the energy wavelength to be $\varepsilon_I = eE\Delta z \approx 18.5$ eV. This contrasts with the *indirect* determination of $\varepsilon_I \approx 18$ eV from the Franck-Hertz experiment (see Figs. 4 and 5), which may also suffer from the *intrusive* effect of the grid. Of course, the wavelengths measured in the two experiments are not expected to coincide exactly, since the photon flux technique does not reflect excitation of atoms to metastable states, whereas the Franck-Hertz measurement includes the effects of *all* collision processes. Note that all quantities in both experiments depend upon the electric field $E = U/d$ and the gas number density n_0 through the *reduced field* E/n_0 (units 1 Townsend = 1 Td = 10^{-21} V m^2).

Fletcher and Purdie discussed their results in terms of quantised energy levels of the neon atom (Tab. 2), and concluded that some weighting of the respective cross sections would be required in order to explain the measured energy wavelength of $\varepsilon_I = 18.5$ eV.

2.5.2 *Argon*

A similar conclusion can be reached for argon, where Fletcher's measured value of $\varepsilon_I = 13.0$ eV [11] does not correspond to any single atomic energy level. It is interesting to note that this is consistent with the voltage wavelength $\Delta U \approx 12 \pm 1$ V which may be extracted from the Franck-Hertz I_A-U data of Magyar et al. [61] for argon, as well as the energy wavelength $\varepsilon_I = 12$ eV of their simulated periodic structures in the drift region.

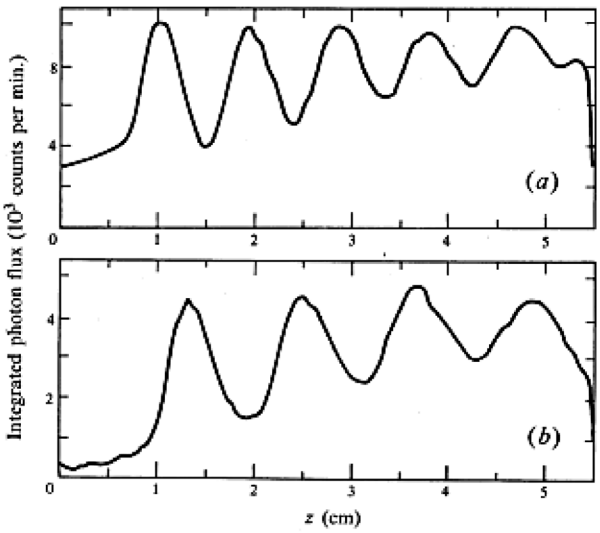

Fig. 6. Measurements of photon flux as a function of inter-electrode distance z arising from de-excitation of atoms in a steady state Townsend discharge with neon, for a reduced electric field $E/n_0 = 30.4$ Td. Gas pressures are (a) $p = 266$ Pa and (b) $p = 254$ Pa (after Fletcher and Purdie [12], http://www.publish.csiro.au/nid/78/paper/PH870383.htm, reproduced with the permission of CSIRO).

2.5.3 *Helium*

References [11,12] detail observations of periodic structures in helium, but we have not been able to find any reports in the literature on a conventional Franck-Hertz experiment using this gas.

As with the Franck-Hertz experiment, the same fundamental question emerges: How do we connect measured wavelengths ΔU and ε_I in the Franck-Hertz and SST experiments respectively, with atomic energy levels? The prescription is provided by rigorous theoretical analysis and is, as we shall see, the same for both experiments.

3 Preliminary theoretical considerations

3.1 Options for a theoretical description

3.1.1 *Mean free path analysis*

Although there have been attempts to analyse the Franck-Hertz experiment in terms of mean free paths [63], this approach is too crude to be of much help. As with modern-day analysis of electron and ion swarms, it is more productive to use momentum transfer theory [64,65]. This forms the basis of the fluid equation approach discussed more fully in Section 5.

3.1.2 *The diffusion equation*

Many electron and ion drift tube experiments [1,13–16] operate in the hydrodynamic regime [66], and may be characterised by mobility and diffusion coefficients, μ and D_L, respectively. These experiments may then be analysed using the diffusion equation, which for plane parallel geometry is:

$$\left(\partial_t + \mu E\, \partial_z - D_L \partial_z^2\right) n = 0, \tag{2}$$

where $n(z,t)$ is the electron number density at position z and time t. However, in both the Franck-Hertz and SST experiments, a steady state exists, i.e., $\partial_t n = 0$, and it is straightforward to show that equation (2) has completely unphysical solutions (see also p. 171 of Ref. [65]), and otherwise has no chance of explaining the formation of periodic structures in the drift region of Figure 1. This simply reflects the fact that these experiments are inherently non-hydrodynamic, and that another means of analysis must be sought.

3.1.3 *Boltzmann equation solution*

In Section 4 we show how the methods of non-equilibrium statistical mechanics may be applied to the Franck-Hertz and SST experiments. Specifically we solve Boltzmann's kinetic equation in phase space [40,41,64–66] for the electron phase space distribution function $f(z, \mathbf{v})$. Properties of physical interest then follow as velocity averages, and the procedure furnishes a complete and rigorous description of electron periodic structures in the drift region.

3.1.4 *Monte Carlo simulation*

In gaseous electronics, Monte Carlo simulation is a popular alternative to solving the Boltzmann equation [12,60,61] (it is interesting to note that there is a school of thought which equates Monte Carlo simulation with solving the Boltzmann equation, but our view is that the two approaches are quite distinct). The method is particularly effective in dealing with boundaries and realistic geometry, which is usually the case with non-hydrodynamic discharges. These may pose difficulties for solution of the Boltzmann equation. The disadvantage of the Monte Carlo approach is that it can be very time-consuming.

3.1.5 *Fluid modelling*

Both Boltzmann equation solutions and Monte Carlo simulations offer a rigorous means of analysis, but are computationally intensive and in the case of the latter, often time-consuming. Neither is particularly conducive to physical insight. Fluid modelling [67,68] on the other hand offers an alternative physically tenable, semi-quantitative, macroscopic description through three balance (or "moment") equations, for number density n, average velocity $\mathbf{v}$ and average energy ε. These equations are generated by taking appropriate velocity moments of Boltzmann's kinetic equation, followed by approximation of the collision terms, e.g., through momentum transfer theory [64,65], along with an appropriate ansatz to close the system of moment equations. Application of these equations to the Franck-Hertz drift region gives a good estimate of the wavelength Δz of the observed periodic structures [67].

3.2 Why the experiment seems to select only certain energy levels

Full details of the fluid model will be given in Section 5 and, as we shall see, the effect of inelastic collisions enters into the energy balance equation through the quantity

$$\Omega(\varepsilon) = \frac{m_0}{2m\sigma_m(\varepsilon)} \sum_i \varepsilon_i \sigma_i(\varepsilon) \exp\left(-\frac{3\varepsilon_i}{2\varepsilon}\right) \tag{3}$$

which is a function of the mean electron energy ε, and the threshold energies and cross sections for excitation of atomic levels, ε_i and σ_i, respectively (see Tabs. 1 and 2 for Hg and Ne, respectively, and Ref. [62] for the corresponding Ar data). The influence of any level i for which σ_i is small may be neglected in the sum, while the exponential term acts to suppress the influence of higher levels, for which $\varepsilon_i > \varepsilon$. As the applied voltage U (and hence E/n_0) increases, ε also increases, allowing higher threshold inelastic channels to contribute to equation (3). However, as discussed in Section 5, the influence of higher levels is suppressed because of a complex interplay between elastic and inelastic processes, and the periodic structure actually *disappears above* a certain critical value of E/n_0 (about 30 Td for Hg) [67]. Then the energy profile $\varepsilon(z)$ becomes monotonic, not oscillatory, and the experiment yields no further useful information.

These two reasons explain why the dominant contribution to the Franck-Hertz experiment with Hg comes from only the *second* excited level with energy 4.89 eV:

(i) The lowest level 4.67 eV is indeed excited, but at a negligibly small rate.
(ii) Even though the third level 5.46 eV may contribute to equation (3) at sufficiently high voltages U, the oscillatory "window" of operational E/n_0 has by then closed.

For Ne, the situation is even more complicated. No single inelastic process dominates (see Tab. 2) and, while equation (3) offers some qualitative insight into the way these processes might be weighted, a quantitative assessment is best left to the more rigorous kinetic theory analysis.

3.3 Internal periodic structures vs. the external current-voltage curve: the essence of the Franck-Hertz experiment

We focus on the drift region between cathode and grid because:

(a) this is where quantum effects at the atomic scale become manifest through the formation of macroscopic periodic structures;

(b) this is also where the electron physics remains poorly understood, often misrepresented and trivialised;
(c) one must fully understand these periodic structures, not only in order to be able to interpret the experimental results, but also to prescribe satisfactory operational conditions, e.g., where to place the grid relative to the cathode and the range of operational voltages and gas pressures; and
(d) the formation of periodic structures lies at the heart of both the Franck-Hertz experiment and the SST experiment of Fletcher and Purdie [11,12]. The *method of observation* of these structures, either indirectly (and intrusively) through the agency of a grid plus retarding field, and projection onto an external current-voltage characteristic, or directly (and non-intrusively) through the photon flux technique, respectively, is quite another matter;
(e) while the experiment furnishes a current-voltage curve over a wide range of voltages, the main interest is confined to its *periodicity*, the peak to peak voltage difference ΔU. The required atomic properties may then be interpreted via the simple relation equation (1), as reasoned previously. The arguments are developed further below;
(f) the full current-voltage curve may well provide additional information, but its detailed shape is influenced by the properties of the grid and the rather complex fields which develop in its vicinity [69]. Since one wishes to measure the properties of the gas atoms, rather than the apparatus which is used to make the measurements, the value of generating the full curve theoretically appears to be very limited, especially when the high computational cost is considered [61].

3.3.1 *Position of the grid*

All these considerations aside, we emphasise that the grid, even if it were to operate ideally and non-intrusively, must be placed far enough downstream from the cathode, so that any "memory" of source properties, specifically, the unknown initial distribution of electron velocities, should be "forgotten". Moreover, as Sigeneger et al. [69] point out, the field structure in the neighbourhood of the grid is really quite complex, so it is something of an idealisation to assume that a uniform field exists over the entire cathode-grid region. In swarm experiments [1,13–16], either the distance of the detector from the source or the gas pressure is increased until measurements become length or pressure independent, indicating that source and "end" effects are negligible. Apart from reference [61], however, Franck-Hertz experiments do not usually have this flexibility, and there is the possibility that both the internal wavelength Δz and peak-to-peak voltage difference ΔU may be "contaminated" by the source or end effects.

3.3.2 *Anode current model*

With these considerations in mind, we assume for present purposes that:

(i) voltages and gas pressures are such that $E/n_0 = U/dn_0$ falls within the operational window for periodic structure formation;
(ii) the grid operates non-intrusively;
(iii) the grid is located in the asymptotic region, sufficiently far downstream from the source so that any memory of initial conditions is negligible; and hence
(iv) properties of the electrons at the grid are determined only by electron-atom scattering properties; and
(v) at any given voltage U, the anode current I_A is determined only by the properties of the electrons at the grid.

In our model, the current is assumed to be a monotonic increasing function of the mean energy $\varepsilon(d;U)$ at the grid, if this exceeds the retarding potential, and zero otherwise, i.e.,

$$\begin{aligned} I_A(U) &= F[\varepsilon(d;U)], \quad \text{if } \varepsilon(d;U) > eU_G \\ &= 0 \qquad\qquad\quad \text{if } \varepsilon(d;U) \leqslant eU_G. \end{aligned} \tag{4}$$

However, we do not need to know any detailed property of the function F. It is also implicit that the energy wavelength $\varepsilon_I = eU\Delta z/d$ of the periodic structure is a constant, independent of U, something which is investigated further in Section 4. Increasing the voltage thus reduces Δz, the pattern shrinks overall, and $\varepsilon(d;U)$ is an oscillatory function of U. In particular if, the voltage increase ΔU is prescribed by equation (1), exactly one more oscillation is introduced into the drift region. Hence if the mean energy at the grid was originally a maximum at voltage U, then it is also a maximum at $U + \Delta U$. Equation (4) then implies the same for the anode current, i.e., the peak-to-peak voltage difference in the external current-voltage characteristic is related to the internal energy wavelength by $e\Delta U = \varepsilon_I$, effectively equation (1).

Of course, apart from the question of how closely the actual experiment approximates this idealised behaviour, it remains first and foremost a priority to understand just how ε_I is related to the atomic energy levels. This is addressed in the next two sections.

4 Rigorous kinetic theory analysis

4.1 The distribution function and Boltzmann kinetic equation

The electron phase space distribution function f contains all the information required to explain the behaviour of electrons in the drift region, but how do we obtain it? We cannot simply assume it to be a delta function in $\mathbf{v}$-space (the unphysical text book description), or take it to be a Maxwellian, since the electrons in a Franck-Hertz drift tube are driven far from equilibrium by the electric field. In fact, the *only* way to obtain f is by solving a kinetic equation, which is a balance (or continuity) equation in phase space. For electrons in the plane parallel geometry of Figure 1 it can be written as:

$$\partial_t f + v_z\,\partial_z f + a\,\partial_{v_z} f = -J(f), \tag{5}$$

where $J(f)$ is the net rate of scattering out of a phase space volume element due to collisions between electrons and atoms, and $a = eE/m$ is the acceleration suffered by an electron of charge e, mass m, due to the action of the electric field.

An expression for $J(f)$ for *elastic* electron-atom collisions can be obtained directly from the classical collision operator proposed by Boltzmann in 1872, which incorporates his famous collision hypothesis ("Stosszahlansatz"), and which introduced the arrow of time [40,41].

The classical Boltzmann collision operator was generalized by Wang-Chang et al. [70] to include inelastic collisions, in this case, collisions where an electron excites an atom from quantum state j to k, with corresponding atomic energy levels ε_j and ε_k. The Boltzmann-Wang-Chang et al. collision operator for electron-atom scattering is [65]

$$J(f) = \sum_{j,k} \int [f(z,\mathbf{v}) f_{0j}(v_0) - f(z,\mathbf{v}') f_{0k}(v_0')] \times g\sigma(jk; g\chi) d\hat{\mathbf{g}}' d\mathbf{v}_0, \quad (6)$$

where dashes denote post-collision properties, quantities with subscripts "0" pertain to the atoms, and $\mathbf{g} = \mathbf{v} - \mathbf{v}_0$ is the relative velocity of an electron and an atom. The differential cross section for the process

$$j,\ \mathbf{v},\ \mathbf{v}_0 \rightarrow k,\ \mathbf{v}',\ \mathbf{v}_0'$$

involving scattering into the solid angle $d\hat{\mathbf{g}}' = 2\pi \sin\chi\, d\chi$, is denoted by $\sigma(jk; g\chi)$, where χ is the scattering angle. An elastic collision corresponds to the case where the internal state of the atom remains unaltered, i.e., $j = k$.

The gas is assumed to be in equilibrium at temperature T_0, and hence $f_{0j}(\mathbf{v}_0)$ is a Maxwellian distribution over velocities $\mathbf{v}_0$, and a Boltzmann distribution over internal states j. For the gases used in a typical Franck-Hertz experiment, the energy levels and temperatures are such that $k_B T \ll \varepsilon_k$, and hence virtually all atoms are initially in the ground state, $j = 0$, $\varepsilon_j = 0$. Thus, for practical purposes, the threshold energy for excitation of an atom to state k is simply the energy ε_k of the final state.

The procedure then is to substitute equation (6) into (5), which for the steady state conditions considered in these experiments, $\partial_t f = 0$, yields

$$(v_z\, \partial_z + a\, \partial_{v_z} + J)\, f = 0. \quad (7)$$

Note that it is common in electron kinetic theory to use a kinetic equation based on a small mass ratio approximation to the collision operator of equation (6) [65], but this does not substantially affect the results.

4.2 Measurable quantities as velocity moments

After solving the steady state Boltzmann equation (7) for $f(z,\mathbf{v})$ with specified cross sections and atomic properties, all quantities of physical interest then follow as velocity "moments", e.g., the electron number density

$$n(z) = \int f(z,\mathbf{v})\, d\mathbf{v} \quad (8)$$

and the mean electron energy,

$$\varepsilon(z) \equiv \left\langle \frac{1}{2} m v^2 \right\rangle = \frac{1}{n(z)} \int \frac{1}{2} m v^2 f(z,\mathbf{v}) d\mathbf{v}. \quad (9)$$

Broadly speaking, the left hand side is the measurable investigated in experiment, while the right hand side contains information about scattering cross sections and threshold energies of the quantised atoms. The Boltzmann equation therefore provides the link between microscopic and macroscopic properties, and enables a rigorous interpretation of the Franck-Hertz experiment.

Note that these averages may also be obtained from either Monte Carlo simulation or directly from approximate fluid equations as explained below. However, for the moment we focus on the kinetic theory approach, and characterise the problem in terms of an eigenvalue problem.

4.3 Boltzmann eigenvalue problem

Eigenvalue problems occur naturally in kinetic theory [54,55], just as they do elsewhere in physics, notably in quantum mechanics. An important difference from quantum mechanics is that the kinetic theory operators are generally not Hermitian, and hence eigenvalues can be complex. This is the case for the eigenvalue problem corresponding to the Franck-Hertz experiment, and indeed as we shall see, the experiment effectively measures the imaginary part of a particular eigenvalue belonging to the spectrum.

The simplest way of understanding how the eigenvalue problem arises is as follows: the steady state Boltzmann equation (7) is separable in z and $\mathbf{v}$, with possible solutions of the form $f(z,\mathbf{v}) \sim \psi(\mathbf{v}) \exp(Kz)$, where K is a separation constant. The functions $\psi(\mathbf{v})$ and allowed values of K are then found as the eigenfunctions and the eigenvalues, respectively of the problem [30]

$$(K_j v_z + a\, \partial_{v_z} + J)\, \psi_j = 0, \quad (10)$$

where we have added an index j to indicate that the eigenvalue spectrum is generally found to be discrete. The integer $j = 0, 1, 2, \ldots$ orders the allowed "modes" in the following way:

$j = 0$ In general, for particle-conserving collisions (elastic and inelastic collisions) considered in this section, the lowest mode has eigenvalue $K_0 = 0$ and corresponds to the spatially homogeneous (sometimes called "equilibrium") case, which would, in principle, be attained at very large distances from the source, and $\psi_0(\mathbf{v})$ is equilibrium velocity distribution function.

$j > 0$ Eigenvalues generally occur in complex conjugate pairs, but only those with negative real part, i.e.,

$$\mathrm{Re}\{K_j\} = -k_j \quad (11)$$

are taken to ensure the correct asymptotic behaviour at large z. Furthermore it will be taken as implicit that

$$k_1 < k_2 < k_3 < \dots$$

On the other hand, the imaginary part of the eigenvalue is written as:

$$\mathrm{Im}\{K_j\} = 2\pi/\Delta z_j, \tag{12}$$

where Δz_j is the "wavelength" of the jth mode. Thus

$$K_j = -k_j + 2\pi/\Delta z_j.$$

The most general solution $f(z, \mathbf{v})$ of the Boltzmann equation (7) is then a linear superposition of all possible eigenmodes $\sim\psi_j(\mathbf{v})\exp(K_j z)$,

$$f(z, \mathbf{v}) = f_\infty(\mathbf{v}) + \mathrm{Re}\left\{\sum_{j=1}^{\infty} S_j e^{K_j z}\,\psi_j(\mathbf{v})\right\}, \tag{13}$$

where $f_\infty(\mathbf{v}) = S_0\psi_0(\mathbf{v})$, and the coefficients S_j could, if desired, be determined from the distribution function $f(0, \mathbf{v})$ at the source [30], though this is generally not known. Near the source, many terms in the summation equation (13) are generally needed, but sufficiently far downstream, at distances z such that $k_2 z > 1$, the fundamental mode $j = 1$ dominates, and only one eigenvalue,

$$K_1 = -k_1 + i\frac{2\pi}{\Delta z_1}$$

determines the asymptotic distribution function,

$$f(z, \mathbf{v}) \approx f_\infty(\mathbf{v}) + \mathrm{Re}\left\{S_1\psi_1(\mathbf{v})\exp\left[\left(-k_1 + i\frac{2\pi}{\Delta z_1}\right)z\right]\right\}. \tag{14}$$

That is, the physical picture is characterised by a single decay constant k_1 and a single wavelength Δz_1. For simplicity these fundamental properties are written as just k and Δz, respectively in what follows.

The asymptotic expressions for the quantities of physical interest then follow by integrating equation (14) over velocity space, as in (8) and (9):

Number density:

$$n(z) = n_\infty + n_1\exp(-kz)\cos(2\pi z/\Delta z + \varphi_n) + \dots \tag{15a}$$

Mean energy:

$$\varepsilon(z) = \varepsilon_\infty + \varepsilon_1\exp(-kz)\cos(2\pi z/\Delta z + \varphi_\varepsilon) + \dots \tag{15b}$$

To which we add for future reference:
Mean velocity

$$v(z) = v_\infty + v_1\exp(-kz)\cos(2\pi z/\Delta z + \varphi_v) + \dots \tag{15c}$$

The constants n_∞, n_1, ε_∞, ε_1, v_∞ and v_1 are prescribed in terms of appropriate integrals over $\psi_0(\mathbf{v})$ and $\psi_1(\mathbf{v})$, and also depend upon the source coefficients S_0 and S_1 [30], while the φ's are corresponding phase differences. It is clear that the spatial profiles of average electron properties in the asymptotic region are, like the distribution function itself in equation (14), characterised by a single, pure "harmonic" of wavelength Δz, which is an intrinsic property of the gas atoms. Ideally, the grid should be positioned at $z = d$ such that

$$k_2 d > 1, \tag{16}$$

to ensure that contributions from higher modes $j = 2, 3,$ in equation (13) are negligible, and thus to ensure that any possibility of "contamination" from the source is eliminated. Equation (16) can be satisfied if d is chosen to be sufficiently large. Alternatively, since wavenumbers are proportional to gas number density (as discussed below), equation (16) can also be satisfied if gas pressure is high enough.

The above theoretical discussion shows, that like the observations of Fletcher and Purdie [11,12], the *internal* picture in the drift region is one of smoothly varying profiles, with curves in the asymptotic region characterised by unique spatial and energy wavelengths, Δz and

$$\varepsilon_I = eE\Delta z, \tag{17}$$

respectively. This contrasts with the *external* I_A-U characteristic which, even if the grid and retarding field operate ideally, is generally not harmonic, sometimes emphatically so. As can be seen from equation (4), there may be "flat" regions, where $I_A = 0$, something which is evident in the experimental curve for neon shown in Figure 4. However, this is not of concern, since in practice one is interested in measuring only the voltage difference ΔU between maximum current peaks, and this furnishes the fundamental property ε_I through equation (1).

To conclude this section, we make a few brief remarks on scaling. Since the collision operator J in equation (7) is proportional to n_0, then properties in the drift region depend upon the field $E = U/d$ through the reduced field $E/n_0 = U/(n_0 d)$, and upon distance though $n_0 z$. Similarly eigenvalues in equation (10) depend upon E/n_0 and scale with number density n_0.

4.4 Computational procedures

The first step in solving the eigenvalue problem of equation (10) is to extract the directional dependence of the eigenfunctions in velocity space. Since there is axial symmetry about the field direction, all properties depend only upon the angle θ between $\mathbf{v}$ and the z-axis, i.e., $\Psi_n(\mathbf{v}) = \Psi_n(v, \theta)$, and the eigenfunctions may be decomposed through an expansion in Legendre polynomials. In principle, the expansion is infinite, but in practice, only a finite number of terms can be considered, and thus we write for the nth eigenfunction,

$$\Psi_n(\mathbf{v}) \approx \sum_{l=0}^{l_{\max}} \Psi_{n,l}(v)P_l(\cos\theta). \tag{18}$$

The upper limit $l_{\max}$ on the l-summation is incremented successively until some accuracy criterion is met, in our work convergence to generally within 1% or so. For low E/n_0, electrons undergo predominantly *elastic* collisions which randomise directions of electron velocity, and the distribution function and eigenfunctions are nearly isotropic in **v**-space. The expansion converges quickly and $l_{\max} = 1$ (the so-called *two-term approximation* [65]) is usually sufficient to give mean energy to better than 1% accuracy. However, when E/n_0 is larger, inelastic collisions become important and enhance anisotropy of f in **v**-space. Then $l_{\max} > 1$ (so-called multi-term analysis) is required to find average quantities to comparable accuracy.

The next step is to represent the coefficients $\Psi_{n,l}(v)$ in speed (or energy) space, and here there are a number of possibilities. One could, for example, represent the function on a finite mesh of speeds or, as in reference [30], expand $\Psi_{n,l}(v)$ in terms of Sonine (generalised Laguerre) polynomials about a Maxwellian weight function with an arbitrary, adjustable temperature, generalising the "two-temperature" method of Mason and McDaniel [64]. Note that the combination of a Sonine polynomial and a spherical harmonic is called a Burnett function, and that the Burnett function representation of the Boltzmann equation provides a basis commonly used for analysing both ions and electrons in gases [64,65].

In addition to investigating the asymptotic regime downstream from the source through eigenvalue problem equation (10), the complete Boltzmann equation (7) has been solved by Winkler et al. [47–49,69] and Li et al. [30,56] over the entire region between source and anode. This requires information about the distribution function $f(0, \mathbf{v})$ at the source and there is also a constraint at large distances,

$$f(z, \mathbf{v}) \to S_0 \psi_0(\mathbf{v}) \quad \text{as} \quad z \to \infty, \tag{19}$$

where ψ_0 is the eigenfunction corresponding to zero eigenvalue. Note that the value of f at any boundary can strictly speaking be specified only in the *half-space* $v_z > 0$, for otherwise there would be an over-specification of the boundary conditions [71]. Such a condition cannot be rigorously imposed for representations of $f(0, \mathbf{v})$ in terms of a finite number of Legendre polynomials, and therefore, as an approximation, we specify only *half* the spherical harmonic expansion coefficients, $f^{(l)}(0, v)$, for $l = 1, 3, 5, \ldots$, while the even coefficients are specified on the upper spatial bound (anode) [30]. Even then, since little is known about the source itself the coefficients S_j in equation (13) cannot be found unless further assumptions are made about $f(0, \mathbf{v})$ [56].

After fixing the boundary conditions, the solution of Li et al. [30,56] proceeds as follows:

(i) as before, $f(z, \mathbf{v})$ is represented in velocity space by an expansion in Burnett functions; and then

(ii) $f(z, \mathbf{v})$ is represented on a mesh of points z_i between source and anode, using a second order finite difference representation of the spatial derivative in equation (7);

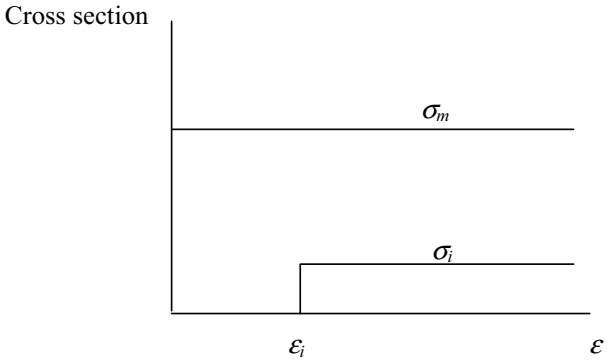

Fig. 7. Cross sections for a model gas with parameters prescribed in the text.

(iii) the resulting (large order) matrix representation of the Boltzmann equation in phase space is then solved after truncation to finite size. The dimension is increased incrementally until some pre-assigned convergence criterion is satisfied, typically 1% or so for the average electron properties (15).

In contrast, Winkler et al. [47–49,69] use the *total* energy $1/2mv^2 – eUz$ as an independent coordinate and discretise accordingly. While one might wish to discuss the computational efficiencies of the respective procedures, obviously an important practical consideration, there is no difference in principle.

4.5 Numerical examples

In this section we summarise the kinetic theory calculations of Li et al. [30,56] for electrons in a model gas and mercury vapour, and the results of White et al. [60] for electrons in neon, calculated using both Monte Carlo simulation and kinetic theory. Results are shown as a function of the reduced field, E/n_0, in units of Townsend (Td).

4.5.1 *Constant cross section model gas*

Li et al. [30,56] solved equations (7) and (10) for a model gas with constant elastic cross section σ_m and one inelastic channel with cross section σ_I constant above the threshold energy ε_i, as shown in Figure 7. The model parameters are $T_0 = 0$ K, $m_0 = 4$ a.m.u. and $\sigma_m = 6$ A^2, with $\sigma_i = 0.1$ A^2, $\varepsilon_i = 2$ eV, $E/n_0 = 9$ Td unless otherwise stipulated.

In the following diagrams, lengths are scaled according to a representative mean free path $\lambda = (\sqrt{2} n_0 \sigma_0)^{-1}$, where $\sigma_0 = 1$ A^2 is a nominal cross section. Thus distances from the cathode are measured in terms of z/λ, while the dimensionless form of the fundamental eigenvalue is

$$K_1^* = K_1 \lambda \tag{20}$$

from which it follows that $\mathrm{Re}(K_1^*) = \lambda\ \mathrm{Re}(K_1) = -\lambda k_1$ and $\mathrm{Im}(K_I^*) = \lambda 2\pi/\Delta z$. The energy wavelength (17) may then be written in terms of a scaled wavelength as:

$$\varepsilon_I(\mathrm{eV}) = 0.0707 \left(\frac{E}{n_0}\right)_{\mathrm{Td}} \frac{\Delta z}{\lambda} \tag{21}$$

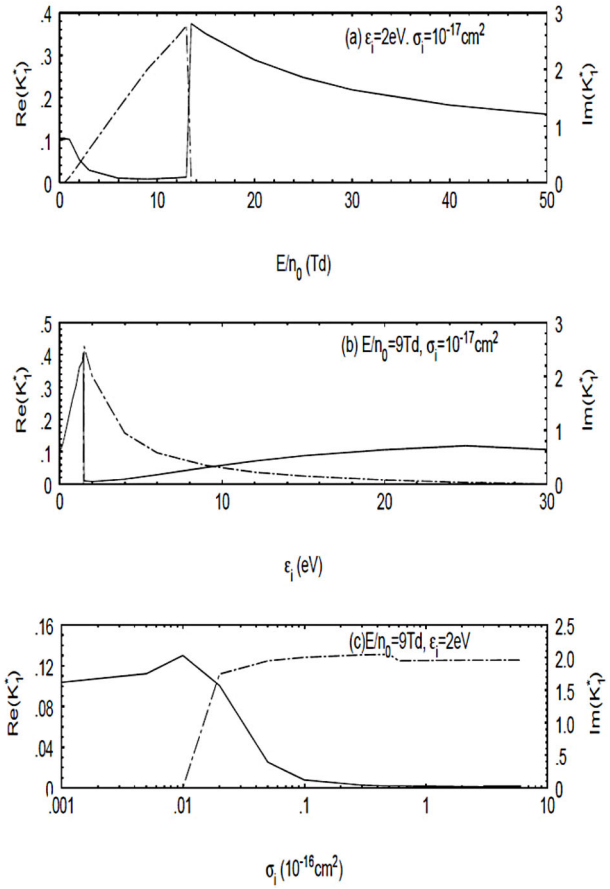

Fig. 8. The (negative of the) real (full line) and imaginary (dotted line) parts of the dimensionless fundamental eigenvalue (20) as a function of: (i) reduced electric field; (ii) threshold energy and (iii) inelastic cross section amplitude, for the step function model of Figure 7. Distances are normalised according to the wavelength λ defined in the text (after Refs. [30,56]).

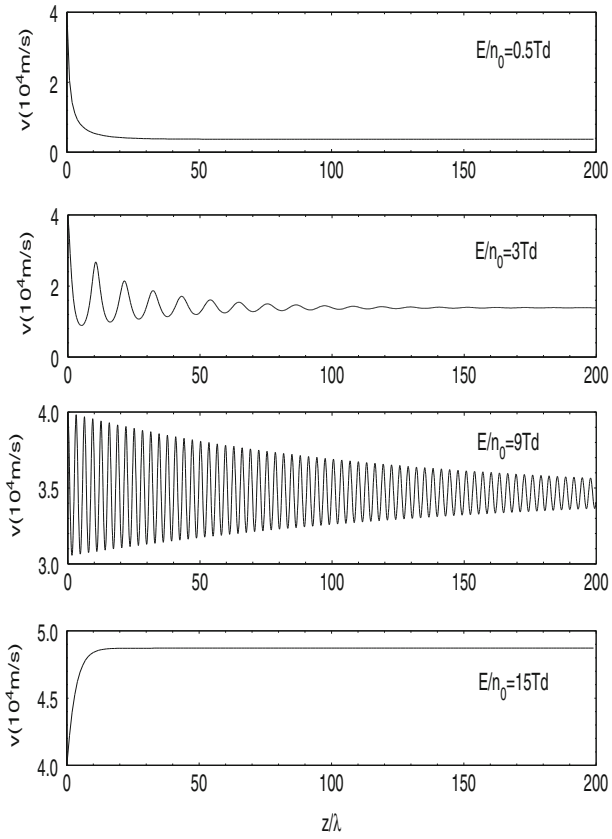

Fig. 9. Spatial profiles of average velocity for electrons in a model gas governed by a step function collision model of Figure 7, for a range of reduced fields [30,56].

or equivalently

$$\mathrm{Im}(K_I^*) = 0.444(E/n_0)_{\mathrm{Td}}/\varepsilon_I. \qquad (22)$$

Figure 8 illustrates the way in which the real and imaginary parts of K_1^* vary with each of the model parameters. In particular, it can be seen that $\mathrm{Re}(K_1^*)$ is small within a "window" of reduced fields 0.5 Td $< E/n_0 <$ 13 Td, and $\mathrm{Im}(K_1^*)$ is proportional to E/n_0. For a fixed value of E/n_0 within the window, $\mathrm{Im}(K_1^*)$ is inversely proportional to ε_i, which is consistent with equation (22) and $\varepsilon_I \approx \varepsilon_i$. This is mirrored in Figure 9, which shows how a periodic structure in average velocity develops and abruptly vanishes as E/n_0 increases from just below the window, to just above. Values of the dimensionless wavelength $\Delta z/\lambda$ obtained from these curves may be substituted into equation (17) to yield an energy wavelength $\varepsilon_I \approx \varepsilon_i = 2$ eV. Here the model atom has only one energy level and there is no possible ambiguity in interpreting the energy wavelength. The last diagram in Figure 8 shows that $\mathrm{Im}(K_I^*)$ increases and then saturates with increasing inelastic cross section. These model gas results provide a prototype for subsequent investigations for real gases. The fluid model discussed in Section 5 enables us to understand the origin of the window phenomenon.

4.5.2 *Mercury vapour*

Eigenvalue method – the asymptotic regime

We now employ the eigenvalue technique for electrons in mercury gas, as originally used by Franck and Hertz [4], with the England, Elford-Hanne cross sections [29,59] as shown in Figure 3. To ensure an accuracy of a few percent in average quantities, we require $l_{\max} = 2$ in equation (18), and Sonine polynomials up to order 10. Results are shown in Figure 10 for the mean energy for a range of values of E/n_0 consistent with experiment. At $E/n_0 = 5$ Td, the dimensionless wavelength is found to be $\Delta z/\lambda \approx 14$ which, with (21), gives an energy wavelength $\varepsilon_I \approx 4.9$ eV, consistent with the $6\,{}^1\mathrm{S}_0 \rightarrow 6\,{}^3\mathrm{P}_1$ transition, and with ΔU as determined from the current-voltage curve Figure 2. The reason that the experiment (and also the theoretical calculations) "selects" this process from amongst the other possible transitions has been explained in Section 3.2.

These calculations include the effect of elastic collisions through the momentum transfer cross section σ_m, as measured by England and Elford [29]. While this is

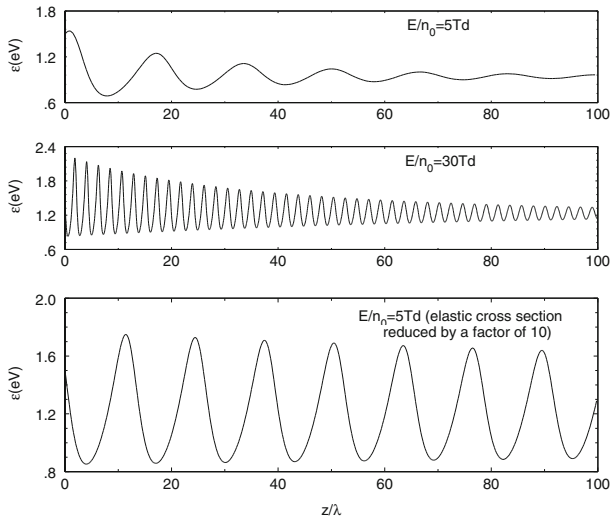

Fig. 10. Spatial profiles of mean energy for electrons in mercury vapour for a range of E/n_0 realised in the Franck-Hertz experiment, and calculated using the eigenfunction method. Although these results strictly speaking hold in the asymptotic region, far downstream from the source, we have, for convenience, drawn the profiles as if they covered the entire region. Figure taken from references [30,56].

clearly enormous, the traditional discussion neglects such collisions entirely, in effect setting $\sigma_m = 0$. Does a drastic assumption like this make any difference to what would be measured in an experiment? The answer may be found in the last diagram of Figure 10, which shows what happens to the mean energy profile when σ_m is reduced by a factor of 10 from that shown in Figure 3. The amplitude of oscillations is markedly increased, and damping is also significantly reduced. Significantly, the *wavelength* is somewhat reduced, and ε_I now lies below 4.9 eV. By virtue of equation (1), the value of ΔU measured in an experiment would also be expected to be *less* than 4.9 V. Although inelastic collisions play the dominant role in determining the wavelength, elastic collisions obviously nevertheless play a small, but significant role in determining the measured value of ΔU.

4.5.3 *Neon*

Winkler et al. [47–49] were the first to investigate periodic structures in neon through solution of Boltzmann's equation, but made no connection with either the Franck-Hertz or SST experiments. Fletcher and Purdie [12] complemented their SST experimental measurements with a Monte Carlo simulation, and remarked on the sensitivity of the results to the choice of cross section set. In this section, we summarise the results of White et al. [60], who investigated neon using both Boltzmann equation and Monte Carlo simulation, based on the set of (e, Ne) cross-sections shown in Figure 11. Elastic scattering is accounted for through the momentum transfer cross-section, and allowance is made for anisotropic scattering, while all inelastic cross-sections including ionization, are assumed

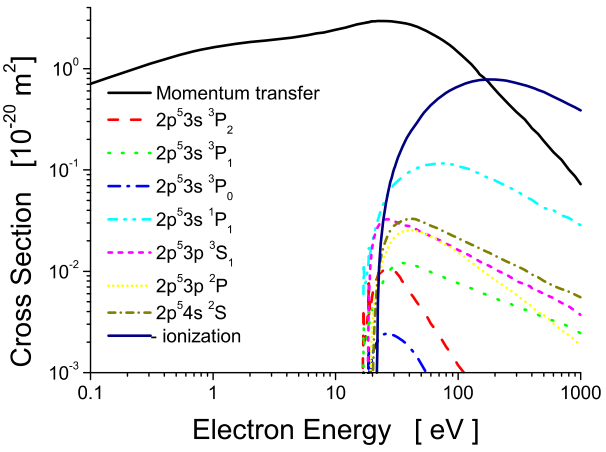

Fig. 11. The electron impact cross-sections for neon as compiled in reference [60]. See legend for the details of the scattering processes.

isotropic. The temperature is fixed at 293 K for all simulations and calculations.

Figure 12 shows profiles obtained from a Monte Carlo simulation [60] in which electrons are released into neon gas with a mono-energetic distribution at 1 eV. For E/n_0 below 2 Td, elastic collisions dominate, and the profile is monotonic. Above about 3 Td, inelastic processes involving excitation of neon atoms to higher energy levels become significant, and an oscillatory profile develops. A further increase of field above 50 Td results in a monotonic profile once more. The physical origin of this "window" is explained in Section 5.

Figure 13 shows $\mathrm{Im}(K_I^*) = \lambda 2\pi/\Delta z$ calculated from wavelengths $\Delta z/\lambda$ estimated from the Monte Carlo profiles of Figure 12, as compared with the corresponding numbers calculated from the Boltzmann eigenvalue problem equation (10). In the Boltzmann equation solution, we have treated ionization as an electron conserving process (i.e., the ejected electron is ignored) while for the Monte Carlo simulation it has been treated exactly. For this reason $\mathrm{Im}(K_1^*)$ is somewhat smaller for the Monte Carlo simulation, or equivalently, the wavelength is larger than for the Boltzmann calculation. This is because treating ionization exactly means that any excess energy after a collision is shared between the ejected and scattered electron. Consequently, on average, the scattered and ejected electrons must travel further to gain sufficient energy from the field to again excite a neon atom, effectively increasing the wavelength. On the other hand if, as in the Boltzmann calculation shown in Figure 13, ionisation is treated as just another inelastic process, there is no such energy dilution, and the wavelength is smaller.

The energy wavelength ε_I is found from the Boltzmann analysis to be 18.8 ± 0.1 eV, and 19.0 ± 0.2 eV from the Monte Carlo simulation. Our Franck-Hertz experimental result (Fig. 4) and equation (1) together give $\varepsilon_I = 18 \pm 1$ eV. Fletcher and Purdie find a somewhat lower value of 18.5 eV in their photon flux experiment [12]. None of these numbers coincide with any particular neon energy

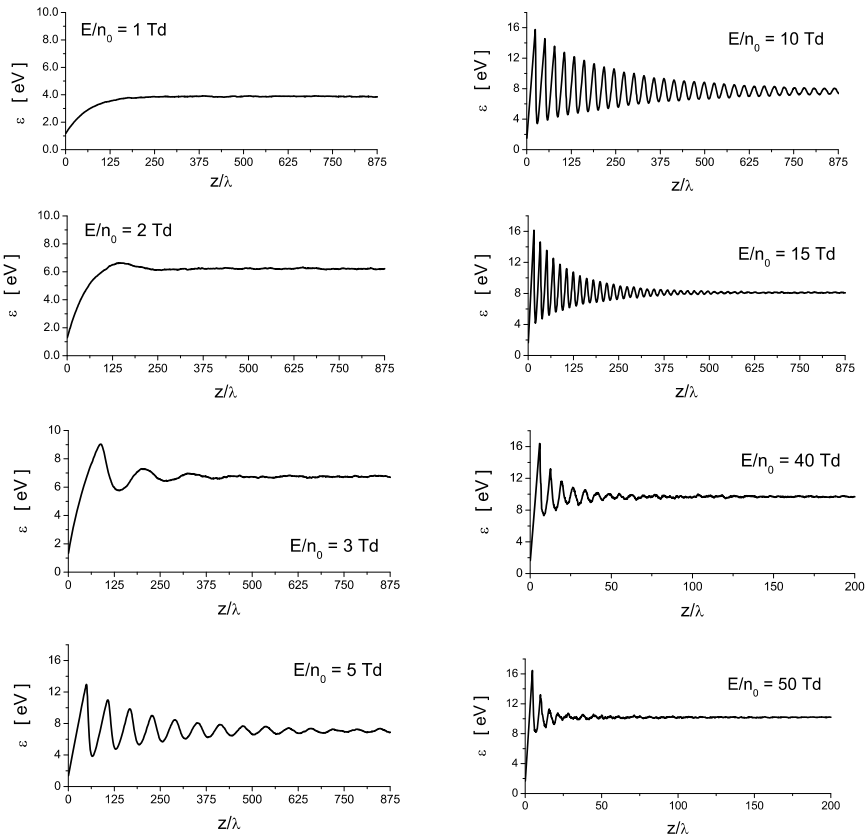

Fig. 12. Spatial relaxation of electrons in Neon for a range of applied reduced electric fields as found through Monte Carlo simulation [60].

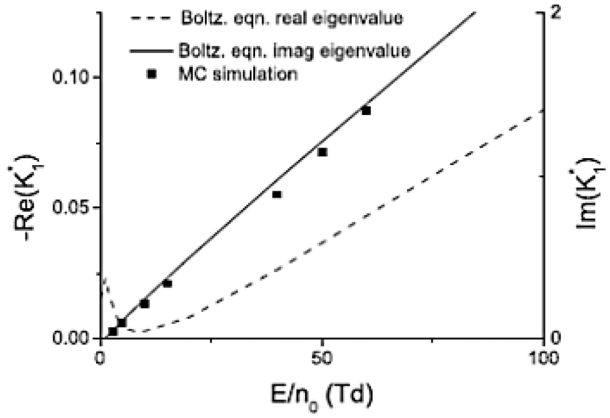

Fig. 13. Variation of the real and imaginary parts of the dimensionless fundamental eigenvalue K_1^* with E/n_0 for electrons in neon, as calculated from solution of the Boltzmann eigenvalue problem equation (10), with the cross sections of Figure 11. The imaginary part increases linearly with E/n_0, consistent with equation (22), while the minimum in the real part of the eigenvalue occurs at around 8 Td, consistent with the oscillatory profile of least damping shown in Figure 12. Also shown are the imaginary part of the eigenvalue obtained from equation (12) and the wavelengths of profiles in Figure 12. Discrepancies between Boltzmann and Monte Carlo results originate from the fact that ionization is treated as just another inelastic process in the former, and as a true non-conservative process in the latter (after White et al. [60]).

level (Fig. 5). The results presented here, both experimental and theoretical, therefore indicate that no particular energy level of neon can be inferred directly from the wavelength of the periodic structures. Figure 11 shows that the excitation thresholds are closely spaced, with cross-sections of the similar orders of magnitude. The best that can be said is that the measured or calculated value of ε_I is the result of a weighted average of the various inelastic processes. It is interesting to note that Fletcher and Purdie [12] also performed a Monte Carlo simulation for neon, and remarked on the sensitivity of the value of ε_I thus obtained to the choice of cross sections.

4.5.4 *Other noble gases*

To date, there has not been any solution of the Boltzmann equation for argon, to compare with the experimental results and Monte Carlo simulations of Magyar et al. [61]. In contrast, solutions of the Boltzmann equation by Winkler et al. [47–49] are available for helium and krypton, but we are not aware of any corresponding Franck-Hertz experiment with these gases.

4.5.5 *Methane*

In general, periodic structures are possible only if the energy gap between the ground and first excited states is

sufficiently large. The second diagram in Figure 8 shows for example, that the imaginary part of the fundamental eigenvalue is zero when the threshold energy is very low. For this reason molecular gases are not considered as candidates for the Franck-Hertz experiment, since they generally have many low lying, closely spaced rotational energy levels. Fletcher [11] and Sigeneger and Winkler [49] demonstrated this, experimentally and theoretically, respectively, for N_2.

An exception to the general rule is methane, for which the vibrational states lie only a few tenths of an eV above the ground state, but this is nevertheless sufficient to generate periodic structure formation [72,73]. Methane is particularly interesting, because it has an elastic cross section with a deep Ramsauer minimum, which is responsible for negative differential conductivity, i.e., drift velocities *decreasing* with increasing E/n_0. However, the Ramsauer minimum is not responsible for producing the Franck-Hertz oscillations, as has been suggested [73].

4.5.6 *The effect of a magnetic field*

Drift tube experiments are sometimes conducted with a magnetic field applied at right angles to the electric field, to enable a finer probe of electron-atom or molecule interaction cross sections [74]. In principle, the Franck-Hertz experiment could also be carried out with a magnetic field, and theoretical investigations by Li et al. [75] and Dujko et al. [76] indicate some very interesting effects. Thus, for example, oscillations may be enhanced or suppressed by the magnetic field, and the operational "window" of the Franck-Hertz experiment modified accordingly. The kinetic theory in this case is much more difficult, as the electric field direction is no longer an axis of symmetry, and the simple Legendre polynomial expansion equation (18) has to be replaced by an expansion in spherical harmonics.

4.5.7 *The influence of ionisation – Lucas-Saelee model*

In many investigations of electron swarms in gases and plasmas ionisation is treated as just another inelastic process. The cross section model of Lucas and Saelee [77] was constructed specifically to test the accuracy of such an assumption. Li et al. [72] and Dujko et al. [78] demonstrated that the assumption leads to errors in the periodic structure profiles, the physical origin of which were detailed above for the neon calculations (see Fig. 13).

5 Fluid modelling

5.1 The window of operational E/n_0 for periodic structures

It is clear from Section 4 and Figure 9 in particular, that there exist both lower and upper bounds of E/n_0 in which periodic structures develop, and outside this "window" of reduced fields electron properties are monotonic. This has the practical implication that the Franck-Hertz experiment can yield useful information only for a certain range of voltages and gas pressures. While one can understand the reason for the lower bound (the field must be high enough to energise electrons above the lowest energy level of the atom), the reason for the existence of the upper bound is by no means clear, certainly from either the Boltzmann equation solution or Monte Carlo simulations, both of which are purely numerically oriented. For that reason we seek to understand the window phenomenon through the "fluid equation" approach.

5.2 General remarks on fluid modelling

As an alternative to solving the Boltzmann equation (7) in phase space, properties of physical interest, such as the mean electron energy equation (9), may also be obtained directly from a set of approximate moment or balance equations (the terms are used synonymously). At the lowest order, balance equations for particle number, momentum and energy are obtained by multiplying the Boltzmann equation (7) with the functions $\varphi_i(\mathbf{v}) = 1$, $m\mathbf{v}$, $\frac{1}{2}mv^2$ ($i = 1, 2, 3$) and integrating over all particle velocities $\mathbf{v}$. The ith member of the set may be written quite generally as:

$$\partial_z \left(n\langle v_z \varphi_i\rangle\right) - na\langle \partial_{v_z} \varphi_i\rangle = -n\langle J^\dagger(\varphi_i)\rangle \quad (i=1,\,2,\,3) \tag{23}$$

where $J^\dagger$ is the adjoint of the collision operator and $\langle\rangle$ is a velocity space average defined as in equation (9). However, the velocity space operators, v_z and $J^\dagger$ act on $\varphi_i(\mathbf{v})$ to generate new quantities outside the original set. Thus, for example, the first term in the $i = 3$ equation is $\langle v_z\varphi_3\rangle = \langle\frac{1}{2}mv^2 v_z\rangle$, an additional moment called the "energy flux". This could, in principle, be found by forming a higher order moment equation, but further unknown moments would then be introduced, and so on. The three equations must somehow be *closed*, by means of at least one approximation (an "*Ansatz*"), so that they can be solved for the three moments of physical interest. In fact an *Ansatz* to approximate the collision terms $\langle J^\dagger(\varphi_i)\rangle$, called 'momentum transfer theory', has long known in both ion and electron swarm physics [64,65], so only an *Ansatz* for the energy flux is required. It is well established [79] that any such approximation must be physically-based, rather than ad hoc, and benchmarked against established results in order to have any chance of success. Nowhere is this more relevant than for analysis of the Franck-Hertz experiment.

The computational economy associated with the fluid model provides not only quick and reasonably accurate quantitative estimates of quantities of experimental interest, but also the physical insight which is missing from numerical solution of the Boltzmann equation, and Monte Carlo simulations.

5.3 The fluid model

The particle number, momentum and energy balance equations for the electrons in the drift region of Figure 1 are [67]:

$$\frac{\partial \Gamma}{\partial z} = 0 \tag{24}$$

$$\frac{2}{3}\frac{\partial (n\varepsilon)}{\partial z} = neE - nm\nu_m(\varepsilon)v \tag{25}$$

and

$$\frac{-1}{\nu_e}\left(v\frac{\partial \varepsilon}{\partial z} + \frac{2\varepsilon}{3}\frac{\partial v}{\partial z} + \frac{1}{n}\frac{\partial J}{\partial z}\right) = \varepsilon - \frac{3}{2}kT_0 - \frac{1}{2}m_0v^2 + \Omega(\varepsilon) \tag{26}$$

respectively, where all symbols have the same meaning as in references [67,79]. Thus $\Omega = \Sigma_i \varepsilon_i(\vec{\nu}_i - \overleftarrow{\nu}_i)/\nu_e$ is the energy transferred in inelastic collisions during one elastic energy relaxation time [65,78]; Γ is the electron flux; e, m, are the electron charge and mass; m_0, T_0, are the atomic mass and temperature of the gas; k is Boltzmann's constant; n, v, ε, are the electron number density, mean velocity, and mean energy; J is the heat flux; ε_i are inelastic thresholds; and ν_e, ν_m, $\vec{\nu}_i$, $\overleftarrow{\nu}_i$, are average collision frequencies for energy transfer, momentum transfer, inelastic, and superelastic processes, respectively. The elastic collision frequencies are given by $\nu_e = (2m/m_0)\nu_m$, $\nu_m = n_0\,(2\varepsilon/m)^{1/2}\sigma_m$, n_0 being the density of ground state atoms and σ_m the momentum transfer cross section. Boundary conditions are such that v and ε are specified at $z = 0$, and that the spatial derivatives of all quantities vanish as $z \to \infty$.

The collision terms on the right hand side of equations (25) and (26) are calculated according to the lowest order of momentum transfer theory [65,68,78], but otherwise the left hand sides are exact. For present purposes we neglect superelastic collisions, since we are dealing with cases where the energy gap is large compared with kT_0. The averages $\vec{\nu}_i(\varepsilon)$ may be prescribed as in Section 7.2 of reference [65], and then equation (3) is a close approximation to Ω. The so-called "direct substitution method" [80] provides a more accurate, empirically based representation of $\Omega(\varepsilon)$.

Equations (24)–(26) are closed through the heat flux *Ansatz* of reference [79]:

$$J = -\frac{2}{3m}\frac{\partial}{\partial z}\left[\frac{n\xi(\varepsilon)}{\nu_m(\varepsilon)}\right] + \frac{(5-2p)}{3}\frac{nqE\varepsilon}{m\nu_m(\varepsilon)} - \frac{5}{3}\Gamma\varepsilon, \tag{27}$$

in which $p = d\ln\nu_m/d\ln\varepsilon$. For *elastic* collisions we can set $\xi = \alpha_0\varepsilon^2$, where $\alpha_0 \approx 1$, as explained in reference [79], but when inelastic collisions are significant, a more general expression must be prescribed. Since ξ has the dimensions of energy squared, the only way to construct such a function is through some combination of both Ω and ε. In reference [67] an additional, empirical *Ansatz* was made

$$\xi = \alpha_0\varepsilon^2\left[1 + \tfrac{\Omega(\varepsilon)}{\varepsilon}\right]^{-r} \tag{28}$$

where r is an adjustable parameter. This expression is justified through the benchmarking and reduces to the established result [79] in the elastic limit $\Omega \to 0$.

5.4 Asymptotic region: the cubic equation

Again following references [67,79], we consider the asymptotic region, far downstream from the source, where all quantities are assumed to be only slightly perturbed from their equilibrium expressions, e.g.,

$$n\,(z) = n_\infty + n_1e^{Kz}, \tag{29}$$

and similarly for $v(z)$, $\varepsilon(z)$ and $J(z)$. Attention is focussed on the decay constant K, expressed in a terms of a dimensionless wave number κ by

$$K = (3/2)(qE/\varepsilon_\infty)\kappa. \tag{30}$$

Equations (24)–(27) are then linearized in small quantities, and after some algebra, there follow three homogeneous equations in the three unknowns, n_1, v_1, ε_1. This system has a nontrivial solution if and only if the determinant of coefficients vanishes, which is expressed as a cubic equation in κ:

$$\frac{3}{2}\alpha\,(\overline{p} - p - 1)\,\kappa^3 - \left(\frac{3}{2}\alpha\overline{p} - \frac{5}{2}p + p^2\right)\kappa^2 - \left(\gamma - 2p - \frac{7}{2}\right)\kappa + (\gamma + 2p) = 0, \tag{31}$$

in which

$$\overline{p} = \frac{\varepsilon_\infty\xi'(\varepsilon_\infty)}{\xi(\varepsilon_\infty)} = 2 + r(1-\gamma) \tag{32}$$

$$\alpha = \frac{\xi(\varepsilon_\infty)}{\varepsilon_\infty^2} = \alpha_0\left[1 + \frac{\Omega(\varepsilon_\infty)}{\varepsilon_\infty}\right]^{-r} \tag{33}$$

and

$$\gamma = \frac{(1+\Omega')\,\varepsilon_\infty}{\varepsilon_\infty + \Omega - (3/2)kT}. \tag{34}$$

Physically meaningful solutions exist for negative K only (solutions of Eq. (29) must decay at infinity) and therefore we seek roots of equation (31) with $\mathrm{Re}(\kappa) \leqslant 0$. For purely elastic collisions, $\Omega = 0$, γ is a constant equal to 1, and the solutions of equation (31) are always real, i.e., there are no oscillations. When inelastic collisions are important, however, Ω is non-zero, and γ may be sharply peaked, as shown schematically in Figure 14. Solutions of equation (31) are complex when γ exceeds a certain critical value, $\gamma_c > 1$, leading to oscillatory behaviour. The corresponding range of fields for this oscillatory behaviour $(E/n_0)_1 < E/n_0 < (E/n_0)_2$ constitutes the operational "window" for the Franck-Hertz experiment. Note that it is different for different gases, and is controlled by both elastic and inelastic collisions, as explained below.

The fluid model was benchmarked in reference [67] against solutions of the Boltzmann equation for the constant cross section model gas of Section 4.5.1 (see Fig. 7).

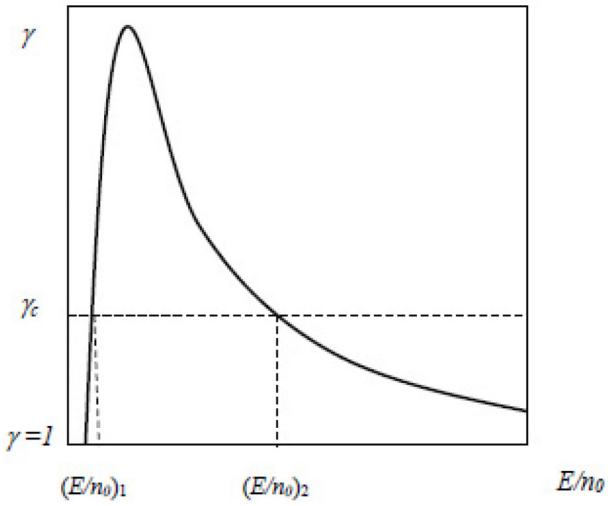

Fig. 14. Schematic representation of the parameter γ defined by equation (34), showing how the "window" of E/n_0 is defined by a certain critical value γ_c (horizontal dashed line), for which the solutions of equation (31) become complex. Note that for purely elastic collisions, $\gamma = 1$ for all E/n_0, the solutions of equation (31) are real, and no oscillatory behaviour is possible.

Solutions of the cubic equation (31) were found for $p = 0.5$, with parameters $\alpha_0 = 0.83$, $r = 0.4$, as discussed in reference [67].

The imaginary part κ_i of the solution of equation (31) gives values of the wavelength

$$\Delta z = \frac{4\pi}{3}\frac{\varepsilon_0}{eE\kappa_i} \tag{35}$$

of periodic structures in the drift region of a Franck-Hertz experiment for the model gas and Hg vapour, which are in good agreement with solutions of the Boltzmann eigenvalue equation (10). This shows that the fluid model may be used as a reliable means of estimating energy wavelengths, if desired. However, the focus of the remainder of this section is on understanding why there are bounds on the reduced field for which these oscillations occur. Note that a good, physically-based heat flux *Ansatz* like equation (27) is critical to the exercise. Certain popular, but deeply flawed, ad hoc expressions for heat flux [81], have no chance of reproducing these effects, even qualitatively.

5.5 Understanding the window phenomenon

We now explore the physical origin of the window phenomenon:

(a) If E/n_0 is so small that inelastic collisions are negligible, such that $\gamma \approx 1 < \gamma_c$, the cubic equation has only real solutions. This is a mathematical reflection of the fact that elastic collisions by themselves provide no physical mechanism for producing oscillations.

(b) As the value of E/n_0 increases, inelastic collisions become significant, and γ increases above unity, as shown in Figure 14. The maximum value $\gamma_{\max}$ to which γ rises is determined by the ratio

$$\rho = \sigma_i/\sigma_e \tag{36}$$

of the inelastic cross section σ_i to the cross section $\sigma_e = (2m/m_0)\sigma_m$ for elastic energy transfer eventually. If this is large enough, $\gamma_{\max}$ lies above the critical value γ_c, and complex solutions of equation (31) become possible, leading to oscillations. For the constant cross section model of Section 4.5.1, $\gamma_c \approx 1.6$, $\gamma_{\max} \approx 30$, and $\rho \sim 2 \times 10^2$.

(c) As E/n_0 is further increased, the *relative* importance of inelastic processes declines: the magnitude of energy loss in elastic collisions continues to increase, but the energy lost in inelastic processes remains fixed. Consequently, after attaining its maximum value, γ falls as E/n_0 increases, and eventually when $\gamma < \gamma_c$ oscillations are no longer possible. This defines the upper bound of the window. For the constant cross section model, the window of reduced fields is predicted by fluid analysis to be 0.5 Td $< E/n_0 <$ 10 Td, in reasonable quantitative agreement with the rigorous Boltzmann analysis (Figs. 8 and 9).

(d) While the value of ρ, and hence $\gamma_{\max}$, is determined in advance by specifying the atomic parameters and cross sections, the corresponding value of γ_c emerges only *after* solution of equation (31). In actual fact, $\gamma_{\max}$ increases and γ_c *decreases* with increasing ρ, producing an expanded window. Conversely, reducing ρ lowers $\gamma_{\max}$ and raises γ_c resulting in a shrinking window. We emphasize that $\gamma_{\max}$ is determined *entirely* by ρ – if this is so small that $\gamma_{\max} < \gamma_c$, then, regardless of the magnitude of the threshold energy ε_i, oscillations cannot occur at *any* E/n_0.

(e) The *width* of the window is actually proportional to the threshold energy ε_i, since the larger its value, the longer the influence of the inelastic collisions lasts (see point (c) above). Conversely, reducing ε_i tends to suppress the width of the window, which is negligible if ε_i is small enough.

(f) It is found that over much of the window the wavelength as calculated from equation (35) is in good agreement with the value found from solution of Boltzmann's equation.

(g) Although the present discussion has been focussed on the constant cross section model, similar reasoning applies to real gases. The cubic equation (31) is solved using real energy-dependent cross sections, and with an energy-dependent parameter p. The operational windows for a Franck-Hertz experiment with Hg is found to be approximately 0.5 Td $< E/n_0 <$ 4 Td in fair agreement with the Boltzmann analysis.

6 Resonances, non-locality and striations

6.1 Spatially varying fields, resonances and non-locality

The Franck-Hertz experiment strictly operates with an externally prescribed *uniform* electric field which drives a

dilute swarm of a single charge species (electrons) from a localized plane source (the cathode) through an atomic gas through to the anode via a grid. The quantized nature of the atoms results in the electrons losing discrete amounts of energy in inelastic collisions, which is reflected on the macroscopic scale through spatial oscillations in mean energy in the drift region of a wavelength $\Delta z \approx \varepsilon_I/eE$, where ε_I is some weighted mean of the threshold energies of the various contributing processes (see Sect. 3.2). These "free" or "natural" modes of oscillation of the electron system may be called "Franck-Hertz waves" in what follows, to distinguish them from oscillations *forced* on the system by a spatially varying field.

Generally speaking, if the mean free path l for collisions between charged particles and gas molecules is comparable with the wavelength l_E of the spatial variations of an externally imposed, harmonically varying field, the response of the system may be *non-local*, that is, physical properties at some point z can be determined by the field at *different* points z'. For light particles such as electrons, l should be interpreted as the mean free path for *energy transfer*, which is several orders of magnitude larger than the mean free path per se. On the other hand, for heavier ions, the two types of mean free paths are comparable. This means that in a *plasma*, consisting of equal numbers of ions and electrons, the response of the electron component to an external field may be non-local, whereas the ions may respond locally.

In addition, *resonances* can be expected if the wavelength of the field is comparable with the Franck-Hertz wavelength, i.e., $l_E \sim \Delta z$. An interesting situation arises if the three length scales are comparable,

$$l \sim l_E \sim \Delta z \tag{37}$$

for then there is a possibility of a *synergy* between resonance and non-local effects.

While an analysis through the Boltzmann equation undoubtedly offers the most rigorous approach [82], fluid analysis offers considerably greater computational economy and more physical insight. Thus the formalism of Section 5 can be readily adapted to space-dependent fields [83], for both model and real cross sections. The response of average electron velocity to a Gaussian-shaped, spatially-dependent perturbing field $E_1(z)$ superimposed on a uniform field E_0 is illustrated in Figure 15. For E_0/n_0 lying within the Franck-Hertz window, resonances occur for those Fourier components of $E_1(z)$ with wavelengths l satisfying equation (37), and significant non-local effects are apparent [83].

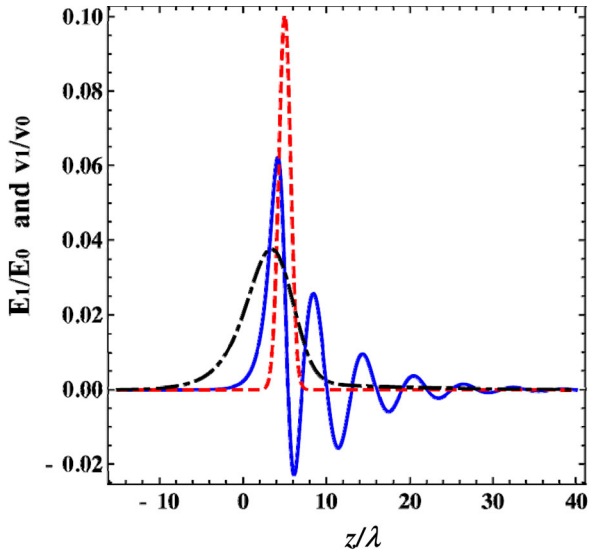

Fig. 15. Perturbations v_1 in electron average velocity in response to a narrow Gaussian spatially-dependent perturbation $E_1(z)$ (red dashed line) centered at $z/\lambda = 5$. Pronounced non-local and resonant effects occur if the unperturbed reduced field E_0/n_0 lies within the Franck-Hertz "window" (blue curve). The black chain curve shows the response if the unperturbed field lies below the window (after Nicoletopoulos et al. [83]). As before $\lambda = (2^{1/2}N\sigma_0)^{-1}$ is a scale length, $\sigma_0 = 10^{-20}$ m^2 is a representative cross section and the collision model is defined as: gas temperature $T_0 = 0$ K, $m_0 = 4$ a.m.u., $\sigma_m = 6$ A^2, and $\sigma_i = 0.1$ A^2 above a threshold of $\varepsilon_i = 2$ eV.

6.2 The path to striations

The above analysis, like much other work in this area (see e.g., Sigeneger and Winkler [82]) is strictly speaking valid for a single species, dilute electron *swarm* in a gas subject to an external field. Nevertheless it can be carried over to deal with a partially ionised *plasma*, consisting of two charged species, ions and electrons, where E_1 is now a self-consistent space charge field, generated by, and in turn acting upon the ion and electron components. Non-locality and resonance effects are then accompanied by screening effects, as characterized by an additional intrinsic scaling parameter, the Debye length l_D.

A three-way synergy between Franck-Hertz waves, non-locality and space-charge fields lies at the heart of *striations*, alternating light and dark fringes, sometimes moving, sometimes stationary, the subject of experimental and theoretical investigation for around 170 years [17]. Although some progress has been made [25], a rigorous theoretical framework has yet to be developed, and consequently there is still no complete physical understanding of this enigmatic phenomenon. Ideally one would solve the Boltzmann kinetic equation for each of the ion and electron components, simultaneously with Poisson's equation. This is a formidable task, however, which has not yet been attempted. Even the fluid approach, which is considerably less computationally demanding, is not a viable option at the time of writing, because a physically-based, benchmarked set of ion fluid equations, suitable for practical application to plasmas, is still to be developed: while general fluid equations for ions have long been available [68], the closure problem is much more difficult than for electrons, where a single *Ansatz* for heat flux (27) suffices. Note that in general, one cannot simply assume an ion fluid model based upon the diffusion equation (2), whose validity is limited.

7 Concluding remarks

This article reviews the Franck-Hertz experiment, starting from the original results for mercury vapour reported 100 years ago, proceeding to neon, and comparing with other experiments in which similar physical processes occur. We examine the conventional interpretation, which has prevailed through several generations of physicists, and show that it is fundamentally flawed. Although the experiment clearly demonstrates atomic quantisation, it is incorrect, in general, to attribute the measured peak-to-peak voltage difference to any one atomic energy level. The exception is mercury vapour, for which a peculiar combination of circumstances produces a fortuitous coincidence between the measurement of 4.9 V and the energy of the second excited state of Hg. From a theoretical perspective, the experiment measures the imaginary part of an eigenvalue of the Boltzmann kinetic equation, which is effectively a sum over atomic levels weighted by the collision cross sections for electron impact excitation of the levels. A fluid model is also discussed, and the origin of the operational window of fields is explained as a complex interplay between elastic and inelastic collisions.

The periodic structures which develop in the drift region of the Franck-Hertz experiment are the natural oscillations of a system of electrons undergoing inelastic collisions in a gas subject to a uniform electric field. If the system is subject to a non-uniform field, resonances at the natural wavelength and non-local effects may occur. Such phenomena also lie at the heart of *striations* long known in low temperature plasmas, but still incompletely understood after 170 years. Solving this long-standing problem would, in the context of the present article, effectively close the circle, since it was investigations of striations, commencing in the mid-nineteenth century, which eventually spawned the seminal gas-discharge experiments around the turn of the century and later, including the work of Franck and Hertz in Berlin. Since it has taken almost 100 years for the Franck-Hertz experiment to be fully understood, perhaps it should not really be surprising that the far more complicated phenomenon of striations should take even longer!

The authors were privileged to work for many years with the late Professor Peter Nicoletopoulos of the Université Libre Bruxelles, who made the study of the Franck-Hertz experiment his life's work. This article is dedicated to him. We also gratefully acknowledge long and fruitful collaboration with Dr Bo Li of the University of Sydney, and Professor Zoran Petrovic and Dr Sasa Dujko of the Institute of Physics in Belgrade. The support of the Paul Scherrer Institute, Switzerland, and the Australian Research Council is gratefully acknowledged.

References

1. L.G.H. Huxley, R.W. Crompton, *The Diffusion and Drift of Electrons in Gases* (Wiley, New York, 1974)
2. S.C. Brown, in *Gaseous Electronics*, edited by M.N. Hirsh, H.J. Oskam (Academic Press, New York, 1978), pp. 1–18
3. A. Müller, Nature **157**, 119 (1946)
4. J. Franck, G. Hertz, Verh. Deutsche Phys. Ges. **16**, 457 (1914)
5. R.E. Robson, M. Hildebrandt, R.D. White, Phys. J. **13**, 43 (2014)
6. G. Holst, E. Oosterhuis, Physica **1**, 78 (1921)
7. M.J. Druyvesteyn, Z. Phys. **73**, 33 (1932)
8. M.J. Druyvesteyn, F.M. Penning, Rev. Mod. Phys. **12**, 87 (1940)
9. J.G.A. Hölscher, Physica **35**, 129 (1967)
10. M. Hayashi, J. Phys. D **15**, 1411 (1982)
11. J. Fletcher, J. Phys. D **18**, 221 (1985)
12. J. Fletcher, P.H. Purdie, Aust. J. Phys. **40**, 383 (1987)
13. R.W. Crompton, Adv. Atom. Mol. Opt. Phys. **33**, 97 (1994)
14. B. Schmidt, K. Berkhan, B. Götz, M. Müller, Phys. Scr. **T53**, 30 (1994)
15. Z.Lj. Petrović, M. Šuvakov, Ž. Nikitović, S. Dujko, O. Šašić, J. Javanović, G. Malović, V. Stojanović, Plasma Sources Sci. Technol. **16**, S1 (2007)
16. Z.Lj. Petrović, S. Dujko, D. Marić, G. Malović, Ž. Nikitović, O. Šašić, J. Jovanović, V. Stojanović, M. Radmilović-Radenović, J. Phys. D **42**, 194002 (2009)
17. M. Abria, Annal. Chim. Phys. **7**, 462 (1843)
18. W.R. Grove, Philos. Trans. R. Soc. London **142**, 87 (1852)
19. G.D. Morgan, Nature **172**, 542 (1953)
20. T. Rùšièka, K. Rohlena, Czech. J. Phys. B **22**, 906 (1972)
21. K. Rohlena, T. Rùšièka, L. Pekárek, Czech. J. Phys. B **22**, 920 (1972)
22. L. Pekárek, Sov. Phys. Uspekhi **11**, 188 (1968)
23. V.I. Kolobov, V.A. Godyak, IEEE Trans. Plasma Sci. **23**, 503 (1995)
24. Yu.B. Golubovskii, A.Yu. Skoblo, A. Wilke, R.V. Kozakov, J. Behnke, V.O. Nekutchaev, Phys. Rev. E **72**, 026414 (2005)
25. V.I. Kolobov, J. Phys. D **39**, R487 (2006)
26. C. Gerthsen, H. Kneser, H. Vogel, *Physik* (Springer-Verlag, Heidelberg, 1982)
27. D. Halliday, R. Resnick, J. Walker, *Fundamentals of Physics* (John Wiley & Sons, 2000)
28. P. Nicoletopoulos, http://users.skynet.be/P.Nicoletopoulos
29. J.P. England, M.T. Elford, Aust. J. Phys. **44**, 647 (1991)
30. R.E. Robson, B. Li, R.D. White, J. Phys. B **33**, 507 (2000)
31. J. Lemmerich, *Aufrecht im Sturm der Zeit: Der Physiker James Franck* (GNT, Diepholz, 2007)
32. F. von Hippel, Phys. Today **63**, 41 (2010)
33. J. Kuczera, *Gustav Hertz* (Teubner Verlagsgesellschaft, Leipzig, 1985)
34. *James Franck-Gustav Hertz, Die Elektronenstreuversuche*, edited by A. Hermann (Ernst Battenberg Verlag, München, 1967)
35. A.C. Melissinos, in *Experiments in Modern Physics* (McGraw-Hill, New York, 1966), pp. 8–17
36. P. Nicoletopoulos, Eur. J. Phys. **23**, 533 (2002)
37. J. Franck, G. Hertz, in *Nobel Lectures, Physics* (Elsevier Publishing Company, 1965), pp. 1922–1946
38. M.J. de Vries, *80 Years of Research at the Philips Natuurkundig Laboratorium 1914–1994* (Pallas Publications, Amsterdam, 2005)

39. *Ludwig Boltzmann (1844-1909)*, edited by I.M. Fasol-Boltzmann, G.L. Fasol (Springer, Wien, New York, 2006)
40. L. Boltzmann, Wiener Berichte **66**, 275 (1872)
41. *The Boltzmann equation and applications*, edited by E.D.G. Cohen, W. Thiring (Springer-Verlag, Wien, 1973)
42. L.M. Chanin, G.D. Rork, Phys. Rev. **132**, 2547 (1963)
43. L.M. Chanin, G.D. Rork, Phys. Rev. A **133**, 1005 (1964)
44. Y. Sakai, H. Tagashira, S. Sakamoto, J. Phys. B **5**, 1010 (1972)
45. H. Sugawara, Y. Sakai, H. Tgashira, J. Phys. D **25**, 1483 (1992)
46. D. Loffhagen, F. Sigeneger, Plasma Sources Sci. Technol. **18**, 034006 (2009)
47. R. Winkler, F. Sigeneger, D. Uhrland, Pure Appl. Chem. **68**, 1065 (1996)
48. R. Winkler, G. Petrov, F. Sigeneger, D. Uhrlandt, Plasma Sources Sci. Technol. **6**, 118 (1997)
49. F. Sigeneger, R. Winkler, Plasma Chem. Plasma Process. **17**, 1 (1997)
50. G. Petrov, R. Winkler, J. Phys. D **30**, 53 (1997)
51. E. Marode, J.P. Boeuf, in *International Conference on Phenomena in Ionized Gase IGPIG 1983, Düsseldorf, Germany, 1983*, p. 206
52. L.D. Tsendin, Plasma Sources Sci. Technol. **4**, 200 (1995)
53. U. Kortshagen, C. Busch, L.D. Tsendin, Plasma Sources Sci. Technol. **5**, 1 (1996)
54. R.E. Robson, in *Gaseous Electronics and its Applications*, edited by R.W. Crompton et al. (Kluwer, Dordrecht, 1997), pp. 89–101
55. H. Date, K. Kondo, S. Yachi, H. Tagashira, J. Phys. D **25**, 1330 (1992)
56. B. Li, Ph.D. thesis, James Cook University, 1999
57. J. Franck, G. Hertz, Phys. Z. **20**, 132 (1919)
58. N. Bohr, Phil. Mag. **30**, 394 (1915)
59. G.F. Hanne, Am. J. Phys. **56**, 696 (1988)
60. R.D. White, R.E. Robson, P. Nicoletopoulos, S. Dujko, Eur. Phys. J. D **66**, 117 (2012)
61. P. Magyar, I. Korolov, Z. Donko, Phys. Rev. E **85**, 056409 (2012)
62. M. Hayashi, NIFS-DATA-72 (2003), www.nifs.ac.jp/report/nifs-data072.html
63. G. Rapior, K. Sengstock, V. Baev, Am. J. Phys. **74**, 423 (2006)
64. E.A. Mason, E.W. McDaniel, *Transport Properties of Ions in Gases* (Wiley, New York, 1988)
65. R.E. Robson, *Introductory Transport Theory for Charged Particles in Gases* (World Scientific, Singapore, 2006)
66. K. Kumar, H.R. Skullerud, R.E. Robson, Aust. J. Phys. **33**, 343 (1980)
67. P. Nicoletopoulos, R.E. Robson, Phys. Rev. Lett. **100**, 124502 (2008)
68. R.E. Robson, J. Chem. Phys. **85**, 4486 (1986)
69. F. Sigeneger, R. Winkler, R.E. Robson, Contr. Plasma Phys. **43**, 178 (2003)
70. C.S. Wang-Chang, G.E. Uhlenbeck, J. de Boer, in *Studies in Statistical Mechanics* (Wiley, New York, 1964), Vol. II, p. 241
71. R.E. Marshak, Phys. Rev. **71**, 443 (1947)
72. B. Li, R.D. White, R.E. Robson, J. Phys. D **35**, 2914 (2002)
73. P. Segur, A. Alkaa, S. Pineau, A. Zahraoui, B. Chouki, C. Moutarde, S. Laffont, Plasma Sources Sci. Technol. **4**, 183 (1995)
74. T. Kunst, B. Gétz, B. Schmidt, Nucl. Instrum. Meth. A **324**, 127 (1993)
75. B. Li, R.E. Robson, R.D. White, Phys. Rev. E **74**, 026405 (2006)
76. S. Dujko, R.D. White, R.E. Robson, Z.Lj. Petrović, Plasma Sources Sci. Technol. **20**, 024013 (2011)
77. J. Lucas, H. Saelee, J. Phys. D **8**, 640 (1975)
78. S. Dujko, R.D. White, Z.Lj. Petrović, J. Phys. D **41**, 24205 (2008)
79. R.E. Robson, R.D. White, Z.Lj. Petrović, Rev. Mod. Phys. **77**, 1303 (2005)
80. P. Nicoletopoulos, R.E. Robson, R.D. White, J. Chem. Phys. **137**, 214112 (2012)
81. M. Surendra, M. Dalvie, Phys. Rev. E **48**, 3914 (1993)
82. F. Sigeneger, R. Winkler, IEEE Trans. Plasma Sci. **27**, 1254 (1999)
83. P. Nicoletopoulos, R.E. Robson, R.D. White, Phys. Rev. E **85**, 046404 (2012)